THE DYNAMIC RELATIONSHIP BETWEEN PERIPHERAL AND CENTRAL NODOSE GANGLION PROJECTIONS: NEUROTROPHIN-4 EXERTS ORGAN-SPECIFIC REGULATION OF VAGAL AFFERENTS

by

Hannah Kathleen Serlin

A Dissertation

Submitted to the Faculty of Purdue University

In Partial Fulfillment of the Requirements for the degree of

Doctor of Philosophy

Department of Psychological Sciences

West Lafayette, Indiana

August 2020

THE PURDUE UNIVERSITY GRADUATE SCHOOL
STATEMENT OF COMMITTEE APPROVAL

Dr. Edward A. Fox, Chair
Department of Psychological Sciences

Dr. Terry L. Powley
Department of Psychological Sciences

Dr. Kimberly K. Buhman
Department of Nutrition Science

Dr. Donna M. Fekete
Department of Biological Sciences

Approved by:
Dr. Jeffrey D. Karpicke

TABLE OF CONTENTS

LIST OF TABLES

LIST OF FIGURES

ABSTRACT

Vagal afferents form the primary gut-to-brain neural axis and are thought to communicate negative feedback signals to the central nervous system to attenuate consummatory behaviors by promoting satiation and possibly satiety. The expansive and fluid nature of the gastrointestinal organs has made it methodologically challenging to decipher the negative feedback signals, and how the signals are disseminated or converged within the central feeding systems. We sought to understand the anatomical relationship and organization between the terminal fields of the peripheral axonal projections and the central axonal projections of gastrointestinal (GI) vagal afferents for clues about what and how information is communicated along the gut-brain axis. Here, we quantified the density and distribution of peripheral and central GI vagal axonal projections in neurotrophin-4 deficient (KO) and control mice. KO mice exhibited a 75 and 55% reduction in small intestinal vagal mucosal afferents, proximally distally, and no significant reduction of mucosal vagal afferents in the stomach, compared to controls. Previous characterization, similarly, reported a >70% reduction in small intestinal vagal muscle afferents and no loss of muscle afferents in the stomach. Centrally, KO mice exhibited an increase in central terminal axonal projections in the medial nucleus tractus solitarius. Our findings support previous hypotheses that neurotrophin-4 exerts an organ-specific regulation of development of gastrointestinal vagal afferents innervation. Furthermore, our findings highlight the dynamic relationship between the peripheral and central axonal projections of vagal afferents.

INTRODUCTION

Obesity is a disease characterized by exceeding amounts of fat in the body and is a major global health problem. Currently, the most efficacious treatment for obesity involves surgically disrupting the gut-to-brain neural feedback (Manning et al., 2015). Despite its efficacy, Roux-en-Y surgery is highly invasive, non-reversible, and 5% of patients experience early complications (Madura & DiBaise, 2012). Overall, Roux-en-Y is a "cookie cutter" procedure being used to treat a disease that on the outside appears to be uniform, but underneath can have a variety of underlying causes from person to person (Lee & Mattson, 2014). Having a greater anatomical and functional understanding of the gut-to-brain neural feedback will lead to more efficacious and less "hammer-like" therapeutic approaches. Furthermore, a greater understanding of the gut-to-brain axis may lead to the identification of early symptoms which may function as warnings in the body-dysregulation tipping point from some excess fat to exceeding amounts. This could help prevent neurological changes which influence the body's defense of higher body weight set points (for set points see: Mrosovsky & Powley, 1977; Keesey & Powley, 2008).

The body itself is composed of nervous tissue that organizes to form local and systemic circuits which send and carry signals within and between different parts of the body. The gastrointestinal tract and the brain form the neural gut-to-brain axis via the Xth cranial nerve; the vagus nerve. The vagus nerve is a bidirectional neural highway composed of afferents and efferents connecting peripheral and central feeding systems involved in regulating energy homeostasis. The vagus plays a role in regulating the bodily functions of ingestion, digestion, and more broadly energy homeostasis, by indirectly and possibly directly (Bohorquez et al., 2018) sensing different gastrointestinal stimuli and communicating that information systemically or reflexively (Chambers et al., 2013; Berthoud & Neuhuber, 2000). What signals are communicated, which signals are communicated systemically or reflexively, and how the information is disseminated or converged within the central feeding systems remains unknown.

These unknowns are in part due to a significant gap in our knowledge about the anatomical structure of the neural gut-to-brain axis. The vagal afferents form the structural highway of communication from the peripheral gastrointestinal organs to the brain. Vagal afferents are unique in that they are pseudo-unipolar neurons. Thus meaning, a single vagal afferent cell body, which resides in the nodose ganglion, has a common branching fiber that bifurcates sending a axonal

projection centrally onto second-order neurons in the caudal-intermediate nucleus tractus solitarius (NTS), area postrema (AP), nucleus ambiguous (NA), and dorsal motor nucleus (DMX) (this cluster of medulla areas, excluding the NA, is referred to as the dorsal vagal complex – DVC) as well as a dendritic-like projection peripherally to a variety of organs including those of the upper gastrointestinal tract (Norgen & Smith, 1988; Berthoud & Neuhuber, 2000).

Vagal gut-to-brain communication occurs through two known means. The first mean is, the centrally projecting vagal afferents synapse onto second-order neurons in the nucleus tractus solitaritus (NTS), where information about the viscera is then distributed throughout the CNS (Davis, 1998). The second mean is, the central axonal projections either connect monosynaptically or through interneurons in the NTS with the vagal efferents in the dorsal motor vagal nucleus forming the neural pathways that mediate vago-vagal reflexes (Takahashi and Owyang, 1997). Both vagal routes of gut-to-brain communication are thought to transmit signals from the gut to the brain about the nutrients ingested (Zittel et al., 1994), gastrointestinal motility (Schwartz and Moran, 1998), and gut immune response (Matteoli et al., 2015).

But, it still remains a mystery as to which vagal fibers in the periphery transmit which signals. In other words, the anatomical structural relationship between the peripheral and central projections and sites of termination of a single nodose ganglion cell body remains unknown. It remains unknown how the site termination of the axonal projection in the periphery influences the site of termination of its' central counterpart. Knowing the relationship between the peripheral and central vagal axonal projections will allow us to investigate the peripheral to central "feeding" circuits as a system, as a whole, which is necessary to 1) build a comprehensive and complete map about what is communicated through the bidirectional gut-to-brain vagal highway, locally, systemically, and reflexively; 2) investigate how information from the peripheral organs is disseminated or converged centrally and onto what second-order neurons in the DVC; and 3) better understand what neurologically goes awry during the development of diseased states such as obesity, gastritis, and Parkinson's Disease. The utility of knowing both the anatomy and function of circuits is highlighted by the significant advancements made in the visual field, notably in the development of specialized, individual therapeutic treatments for the spectrum of underlying causes of visual impairment. Therefore, the aim of the current experiments was to build the anatomical knowledge about the relationship between the peripheral and central vagal afferent axonal projections.

The lack of structural knowledge about the gut-to-brain axis is largely due to a lack of techniques or known molecular marker to selectively investigate, independent of the efferents and other gastrointestinal neural networks, the function and the anatomical organization of the vagal afferents (Fox, 2006). Currently, there is no technique available to selectively label or record from a single nodose ganglion neuronal body and its projections and do so consistently from animal to animal.

Previous researchers have employed a variety of nerve tracing techniques to investigate the topographic relationship between the peripheral and central axonal projections. Norgen & Smith (1988) examined the distribution of retrogradely labeled afferent axons in the DVC by incubating the five major abdominal vagal branches in wheat germ agglutinin (WGA-HRP). More recently, viruses and single-cell RNA sequencing have been employed to explore and map the relationship between the peripheral and central vagal axonal projections (Williams, et al., 2016; Han et al., 2018; Bai et al., 2019; Kupari et al., 2019). While each technique has progressed our understanding, the maps remain incomplete and the relationship between the peripheral and central projections unknown. A lack of characterization and control of the diffuse spread of the different tracers employed has made it difficult to interpret the relationship between the central terminal patterns depicted and peripheral tracer delivery sites (Fox and Powley, 1989). An overall lack of characterization of the peripheral projections labeled with each technique, especially beyond the very most proximal portion of the duodenum, has left maps difficult to interpret. Injection labeling techniques are also inherently variable and dependent on the quality of each injection.

To overcome these obstacles and explore the peripheral and central relationship of vagal axonal projections, we quantified the density and distribution of the peripheral and central vagal afferent terminals of neurotrophin-4 deficient mice (NT-4 KO). Previous characterization of neurotrophin-4 global knock out and knock in mice have revealed the trophic effects of this nerve growth factor on the vagal afferents and have posed this mouse model as a means to investigate the topographic relationship (Fox et al., 2001; Chi et al., 2004).

Previous characterization demonstrated that NT-4 deficient mice exhibit a 50-60% loss of neuronal cell bodies in the nodose ganglion (Fox et al., 2001). Anatomical characterization of the peripheral vagal afferent projections in the gastrointestinal tract of NT-4 deficient mice revealed an almost complete elimination of vagal afferents terminating within the muscle layer of the small

intestine. In stark contrast, the morphology and density of vagal afferents terminating within the muscle layer of stomach were similar to that of wildtype control mice.

Unfortunately, the tracer employed in the original characterization was unable to penetrate the submucosal and mucosal layers in the stomach and small intestine. Therefore, while it was demonstrated that neurotrophin-4 is important for the survival of vagal afferent projections to the muscle layer of the small intestine, it remains unknown if the neurotrophin-4 is similarly important for vagal projections to the mucosa layer of the stomach and/or small intestine. A greater than 70% loss of fiber bundles in the small intestine, but not the stomach, suggested that NT-4 KO mice most likely do exhibit an organ-specific vagal afferent loss (Fox et al., 2001). To investigate if the loss extends into the mucosal layer, we crossed NT-4 KO mice with Nav1.8-cre-; Rosa26R-tdTomato mice to visualize and quantify the density and distribution of the vagal afferent innervation in the mucosa of the stomach and small intestine. We, and others, have previously demonstrated the breadth of labeled nodose ganglion and vagal afferents in the gastrointestinal tract of Nav1.8-cre-; Rosa26R-tdTomato mice (Gautron et al., 2011; Serlin and Fox, 2019).

In the present study, we quantified and characterized the density and distribution of mucosal vagal afferents in stomach and small intestine of NT-4; Nav1.8-cre-; Rosa26R-tdTomato KO and control mice to investigate if the peripheral vagal afferent loss was organ or tissue layer specific. To explore the relationship between the peripheral and central axonal projections, we also quantified and characterized the central projections in the DVC. Through detailed characterization of the loss peripherally, and quantification of how the loss was impacted central projections, we were able to explore the relationship between the peripheral and central vagal axonal projections. We hypothesized that neurotrophin-4 supports GI vagal afferents in an organ-specific manner. If so, we further hypothesized the elimination of vagal innervation in the small intestine would be reflected centrally as a reduction in terminal density in the DVC.

METHODS

Mice Breeding

Mice heterozygous for the Nav1.8-Cre transgene on a C57Bl/6 background (*Scn10atm2(cre)Jnw*) [obtained from Laurent Gautron and Joel Elmquist (University of Texas Southwestern Medical Center) with permission of John Wood (University College London)], and mice heterozygous for the Rosa26R-tdTomato transgene on a mixed B6-129S6 background [(cat no. 007905, Jackson Laboratory, Bar Harbor, ME; [Madisen, 2010 #2510], were bred to homozygosity and maintained for several generations in the laboratory. NT-4 mutant mice (C57/ SvJae-Ntf5tmlJae; -/-) were obtained as a gift from Lino Tessarolo at NIH and maintained for several generations in our laboratory. Nav1.8-Cre, Rosa26r-tdTomato, and NT-4 mutant mice were genotyped by polymerase chain reaction as previously described (Gautron et al., 2011, Jackson Laboratory).

Mice homozygous for the Nav1.8-Cre transgene were bred with homozygous NT-4 mutant mice to produce offspring heterozygous for both the Nav1.8-Cre and NT-4 transgenes (Nav1.8-Cre-/+; NT-4-/-,). In parallel, mice homozygous for the Rosa26r-tdTomato transgene were bred with homozygous NT-4 mutant mice to produce offspring heterozygous for both the Rosa26r-tdTomato and NT-4 transgenes (tdTomato-/+; NT-4-/-). Offspring from each (Nav1.8-Cre-/+;NT-4-/+, tdTomato-/+;NT-4-/+) were then bred to produce offspring heterozygous for both the Nav1.8-Cre and Rosa26r-tdTomato transgenes, and either homozygous mutant (NT-4 KO) or heterozygous (NT-4 HET) for the NT-4 mutant transgene. NT-4 homozygous wildtype mice were not utilized in the current study due to an underrepresentation in the litters. NT-4 HET mice only exhibit approximately an 8% loss of nodose ganglion neurons compared to the 55% loss in NT-4 KO mice (Conover et al., 1995).

Animals

NT-4 KO (n = 10) and NT-4 HET (n = 12) male mice 3.5-4 months were group-housed (5 mice maximum per cage) prior to experiments and maintained at 23°C on a 14:10 hr light:dark schedule with lights on at 0500. Mice had ad libitum access to tap water and food (Envigo Tekland Global Diets 2018, Autoclaved, Crude Protein 18.6%, Fat 6.2%, Carbohydrate 44.2%) unless

stated otherwise. When necessary to facilitate breeding, diets were supplemented with irradiated in-shell sunflower seeds (Advanced Protocol Picolab Natural Sunflower Seeds #5LP8; Purina Mills; [Jugloff, 2006 #2104]. All procedures were conducted in accordance with National Institutes of Health Guide for the Care and Use of Laboratory Animals (eighth edition) and American Association for Accreditation of Laboratory Animal Care guidelines and were approved by the Purdue University Animal Care and Use Committee.

Sacrifice

The transcardial perfusion process was utilized and previously described elsewhere (Serlin Fox, 2019, see Methods 2.4 Tissue preparation). Briefly, mice were deeply anesthetized with Brevital (sodium methohexital, 100 mg/kg, Par Pharmaceutical Companies, Inc., Spring Valley, NY). Mice were transcardially perfused with saline at 4 ml/min at room temperature for 10 min followed by ice cold 4% paraformaldehyde (PF) made in phosphate buffer (PB) for 30 min. The gastrointestinal tract was expanded with ice cold 4% PF in PB during saline perfusion.

Tissue Preparation

Following perfusion with 4% PF, the stomach, small intestine, brain with attached medulla were harvested. All tissue was stored in 4% PF in PB ON at 4oC. The following day, the tissues were flushed with, and transferred to, 15% sucrose in PBS for 2 h at 4oC. Then the tissues were flushed with, and transferred to, 30% sucrose in PBS and stored ON at 4oC.

Small Intestine

Following 30% sucrose in PBS overnight the small intestine was stretched taught (i.e. - exhibiting a slight backwards retraction when tugged) to accurately identify the predetermined proximal-to-distal locations to be collected for sectioning and lengths of small intestine. The collection process for the small intestine has previously been described elsewhere (Serlin & Fox, 2019, see Methods 2.4 Tissue preparation). Briefly, the small intestine was injected to expansion, with a 1:1 mixture of PBS and OCT (Sakura Tissue Tek, Torrance, CA) and the length of the small intestine (distance from the gastroduodenal junction at the mid-pylorus to the ileocecal junction) was measured and used for calculating the locations of the proximal and distal borders of the

duodenum, jejunum, and ileum, using a 1:3:2 ratio, respectively (Duan, 2004; Wang, 2007). Tissue blocks, 1 cm in length, at predetermined collection sites were sutured closed (Figure 1) (3-0 Black Braided Silk, Surgical Specialties Corp., Reading, PA). Each 1 cm block was transferred to a mold (Polysciences, Inc., Peel-A-Way Disposable Embedding Molds, Cat no. 18985) filled with OCT and frozen, using liquid nitrogen and stored at -80oC. A small subset of intestines were harvested and processed as whole mounts.

Stomach

Following 30% sucrose in PBS overnight, the stomach from the proximal corpus (the side of the esophagus between the fundus and corpus) to the pylorus was cross-sectionally divided, using a razor blade, into four equal pieces of tissue; these regions were termed proximal corpus, middle corpus, antrum, and pylorus (Figure 2). The fundus was excluded from analysis because it does not have a mucosa tissue layer. Each cross-sectionally divided piece of tissue was transferred to molds (Sakura, Tissue-Tek Cryomold, Disposable Vinyl Specimen 25mmx20mmx5mm) filled with OCT and frozen, using liquid nitrogen and stored at -80oC.

Medulla

Following 30% sucrose in PBS overnight, using a razor blade, a single cut was made immediately rostral to the cerebellum thus leaving the medulla and cerebellum intact. The cerebellum was then gently dissected off of the medulla. This issue block was transferred to a mold, (Sakura, Tissue-Tek Cryomold, Disposable Vinyl Specimen 25mmx20mmx5mm) with the most anterior tissue face down. The mold was filled with OCT and frozen, using liquid nitrogen and stored at -80oC.

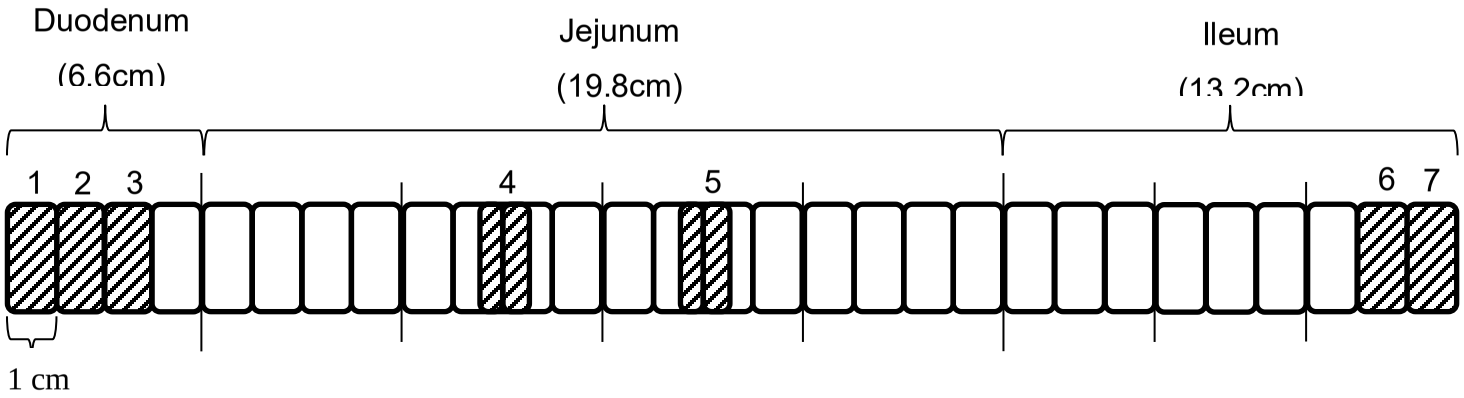

Figure 1. Schematic diagram of the relative location of the 7, 1 cm blocks collected for quantifying mucosal innervation along the length of the entire small intestine (blocks are numbered 1 - 7 from the proximal to the distal small intestine). The duodenum, jejunum and ileum were defined by dividing the entire length of the small intestine according to a 1:3:2 ratio, respectively. It is important to note, because of the method used for harvesting, there were small 1-3mm gaps between consecutively collected 1 cm blocks.

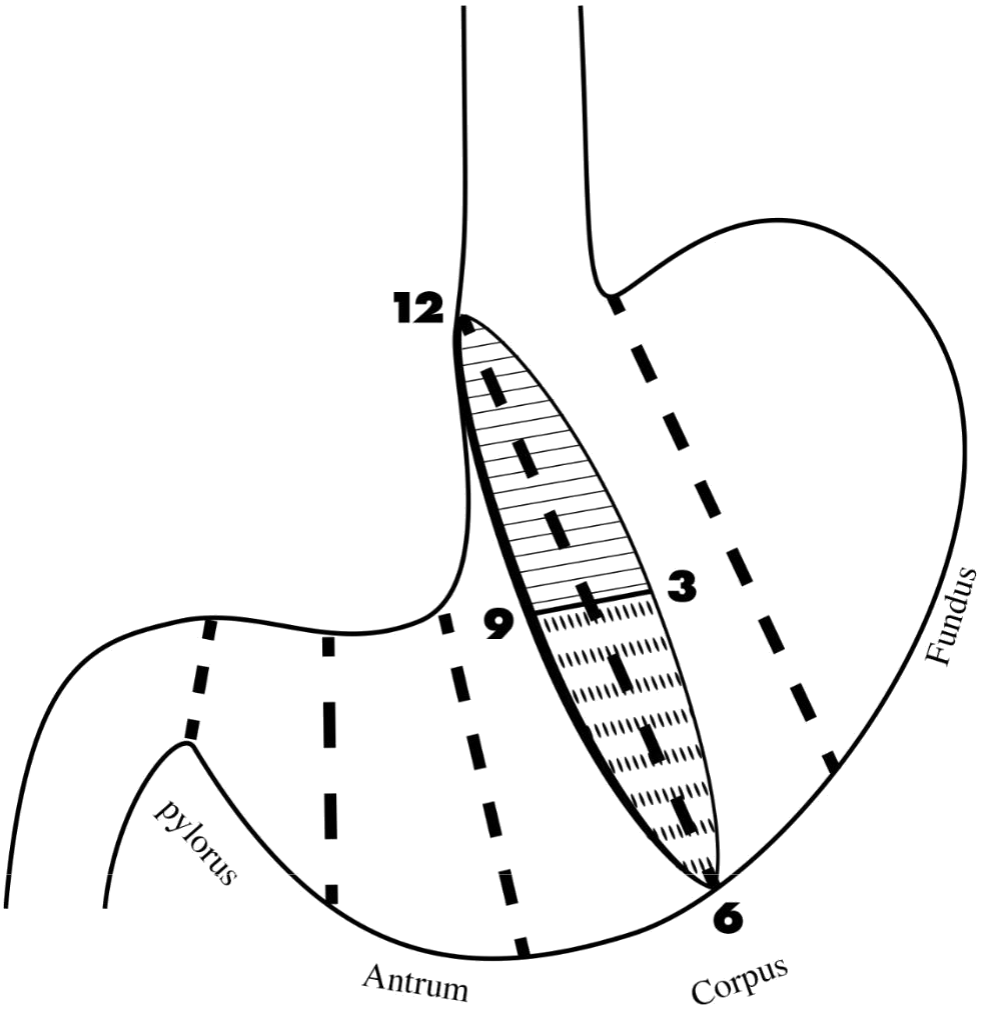

Figure 2. Schematic diagram of the relative location of the 4 regions collected for quantifying mucosal innervation along the length of stomach. The 5 thick dashed vertical lines denote the boundaries of the 4 regions, with the region closets to the fundus and moving left, the regions were labeled as: the proximal corpus, mid-corpus, antrum, and pylorus. The numbers (12, 3, 6, 9) denote the 4 spots along the circular axis in which the number of fibers contacting the basal and apical ends of the mucosal glands were quantified. High noon designates the oral, 3 the dorsal, 6 the aboral, and 9 the ventral spots of quantification. The vertical lines represent quantification around the lesser curvature half, and the polka dots around the greater curvature half.

Immunohistochemistry

All tissue blocks from the small intestine, stomach, and medulla were cross-sectioned at 30 um (i.e. - the medulla was coronally sectioned). The small intestine and stomach tissue blocks were cross-sectioned in an anterior to posterior fashion. Medulla coronal sections were cross-sectioned in an posterior to anterior manner. Stomach and small intestine cross-sections were directly mounted on gelatin-coated slides and processed in a humidified chamber. Medulla coronal cross-sections were processed as free-floating sections in 12-well plates with baskets to aid in the transferring of sections from solution to solution. Medulla sections were processed on a shaker and mounted onto gelatin-coated slides following the last 3x10 min cold PBS washes. All immunohistochemistry was carried out at room temperature to maximize antibody penetration.

The immunohistochemistry process has been described in more detail elsewhere (Serlin & Fox, 2019, see Methods 2.7 Immunostaining of tdTomato-labeled axons and terminals). Briefly, sections were incubated in 4% PF for 15 min, followed by 3x10 min cold PBS washes. Next, sections were incubated with fresh blocking buffer [0.5% phosphate-buffered saline/triton (PBST), 5% normal goat serum (NGS), 0.08% Sodium Azide, 2% bovine serum albumin (BSA)] for 1 hr and then incubated ON with the primary antibody for tdTomato diluted in blocking buffer (1:1500). The following day, sections were washed 3x10 min in cold PBS. Secondary antibody (1:600; Cy3-conjugated AffiniPure Goat Anti-Rabbit IgG stored in glycerol, Jackson ImmunoResearch, 111-165-003) was applied to the tissue sections for 2 hr, followed by 3x10 min cold PBS washes. Sections were cover-slipped with glycerin (Mallinckrodt), sealed with clear nail polish (L.A. Colors, Cat# 72180), and stored in the dark at 4oC. The specificity of this immunostaining protocol was tested each run using the same procedure as described above, except the blocking buffer was not replaced with primary antibody ON. Slides were examined and no non-specific staining was observed on any staining run.

The small subset of small intestines that were harvested as whole mounts, the mucosa and submucosa tissue layers were peeled off leaving just the muscle tissue layers. The muscle tissue layer was then stained as described elsewhere (Fox et al., 2001). Briefly, the mucosa and submucosa of the most proximal 4 cm was separated from the muscle tissue layers. The muscle tissue layer whole mounts were then processed as free-floating whole mounts, stained using DAB (3,3′-Diaminobenzidine), cover-slipped using cytoseal (Richard-Allan Scientific, Cat# 8312-4), and stored in the dark at 4oC.

Quantification of Vagal Afferents

Quantification of tdTomato-labeled vagal afferents was performed blind to group within 48 hr of cover-slipping the tissue sections to minimize fluorescent fading. Quantification of each element was repeated in the same systematic order from animal-to-animal to minimize any order effects on fluorescence fading that could have affected group differences. A 2 mm2 ocular grid composed of ten 0.2 mm x 0.2 mm squares was used to quantify.

Small Intestine

tdtomato-labeled fibers innervating the mucosal (i.e. – crypts and villus) tissue layer, along the longitudinal axis, of the small intestine were quantified. Several criteria had to be met for a small intestine section to be included for quantification and has been described elsewhere (Serlin & Fox, 2019, see Methods 2.8 Quantification of axons, terminals, and mucosal structures). A maximum of 2 sections were quantified at each of the 4 harvesting sites within a 1 cm frozen tissue block for a total of 8. A minimum of 5 sections per frozen tissue block must have met criteria for the quantifications to be included in analysis.

To characterize the pattern and density of vagal afferents 5 features were quantified: the number of axons entering the villus base, the number of terminal branches half-way up the height of the villus, the percentage of crypts in close apposition to tdtomato-labeled fibers, the width of the villus, and the height of the villus. How each measure was defined has been described elsewhere (Serlin & Fox, 2019, see Methods 2.8 Quantification of axons, terminals, and mucosal structures). Briefly, a horizontal gridline was placed at the base of the villus and the number of fibers that crossed the gridline was quantified as the number of axons entering the villus base (*base axons)*. The gridline was then moved mid-way between the basal and apical poles of the villus and the number of fibers that crossed the gridline was quantified as the number of terminal branches half-way up the height of the villus (*terminal branches*). Fiber innervation of the crypts was quantified around the entire circular axis in a bimodal manner (*crypt associated fibers)*; “yes” a fiber contacted a crypt or “no” fibers contacted the crypt. There was no attempt to quantify the amount of fiber contacts per crypt. The height and width of each villus was quantified by the number of grid-boxes. Each grid-box was subdivided into fourths for better accuracy of villus width and height.

Stomach

tdtomato-labeled fibers innervating the mucosal tissue layer, along the circular axis of the stomach were quantified. For a stomach section to be quantified the cross-section must (1) be a fully intact cross-section, (2) no folding or damage that would impede counts, (3) no obvious right to left or top to bottom unevenness of staining, and (4) low background staining. A maximum of 3 sections were quantified at each of the 4 harvesting sites (i.e. – proximal corpus, middle corpus, antrum, pylorus). Ultimately, the most aboral region, the pylorus, was excluded from analysis due to difficulty in meeting these pre-determined quantifications. Given its high importance in the regulation of digestive and ingestive behaviors, future studies should aim to characterize this transition zone between the stomach and small intestine (Sugawara et al., 1969; Powley et al., 2005; Serlin & Fox, 2019).

To characterize the pattern and density of tdtomato-labeled fibers 3 features were quantified. These features included (1) the total number of fibers half-way up the mucosal glands, (2) the number of fibers contacting the basal third of a gastric gland, and (3) the number of fibers contacting the apical third of a gastric gland. The total number of fibers half-way up the mucosal glands was quantified by counting how many fibers contacted a horizontal gridline placed half-way up each gastric gland (i.e. – similar quantification as *terminal branches* in the villi). This measure was quantified around the entire circular axis of each gastric cross-section. The number of fibers at the basal and apical end of a gastric gland was quantified by subdividing each gland into thirds. The number of fibers contacting the gastric gland in its bottom and top third were counted and recorded as their respective measure. This basal and apical pole count was quantified at 12 (oral), 3 (ventral), 6 (aboral), and 9 (dorsal) o'clock around the circular axis (Figure 2). The middle of the ocular grid was placed in line with each location and the glands that were within the left-right boundaries of the grid were quantified.

Medulla

tdtomato-labeled fibers passing through or terminating within the NTS and AP, along the rostral-caudal axis of the medulla (-7.2 to -7.9, see Paxinos et al., 2012 mouse brain atlas) were quantified. Medulla cross-sections were imaged using a spinning-disk confocal microscope (info) and quantified using Image J software (Version 1.51, 2015). To be included in quantification

coronal cross-sections must have been (1) be fully intact, (2) no folding or damage that would impede counts, and (3) no obvious right to left or top to bottom unevenness of staining. Six rostral-caudal levels were pre-determined prior to quantifications (-7.2, -7.3, -7.4, -7.5, -7.6, -7.9 mm anterior-posterior coordinates from bregma based on the mouse brain atlas Paxinos, 2008). This range of anterior-posterior coordinates was selected based on the current knowledge of the neuroanatomy of the termination of afferent input to the NTS (Bradley, 2007; Altschuler et al., 1989; Norgren and Smith; 1988; Bai et al., 2019) and c-fos expression in the NTS following stimulation of the gastrointestinal tract (Emond et al., 2000). The NTS is arbitrarily subdivided 3 rostro-caudal levels; the rostral, intermediate, and caudal NTS and, as a whole, the NTS is thought to follow a topographic rostrocaudal oral to aboral organization (Bradley, 2007; Altschuler et al., 1989; Herbert et al., 1990). The rostral NTS predominately receives gustatory afferent input from the oral cavity (King, 2007), while gastrointestinal afferent input is thought to terminate in the intermediate and caudal NTS (Cutsforth-Gregory et al., 2017). The range selected evenly samples throughout the bulk of the intermediate and caudal NTS.

The pattern and density of tdtomato-labeled fibers in the medulla was characterized by the number of pixels above a pre-set threshold in a pre-determined area. We divided the NTS into medial and lateral sub-regions to more finely investigate if there were any alterations in central vagal afferent axonal projections (Figure 3). Because the transgenic mouse model utilized selectively labels afferent fibers (i.e. – does not label efferents), the outline of the "football shaped" dorsal motor nucleus (DMX) was easy to identify in each cross-section. The outline of the DMX was used as a guide to divide the NTS into medial and lateral sub-regions. At each cross-section the medial NTS was defined as extending from the AP-NTS transition region to the "peak" of the football shaped DMX. The lateral NTS was defined as the lateral boundary of the medial-NTS extending to the end of the continuous label. Previous demarcations of a medial and lateral NTS (Altschuler et al., 1991; Herbert et al., 1990) and insights into the potential patterning of central vagal afferents (Norgen and Smith, 1988) influenced our decision of how to sub-divide the NTS.

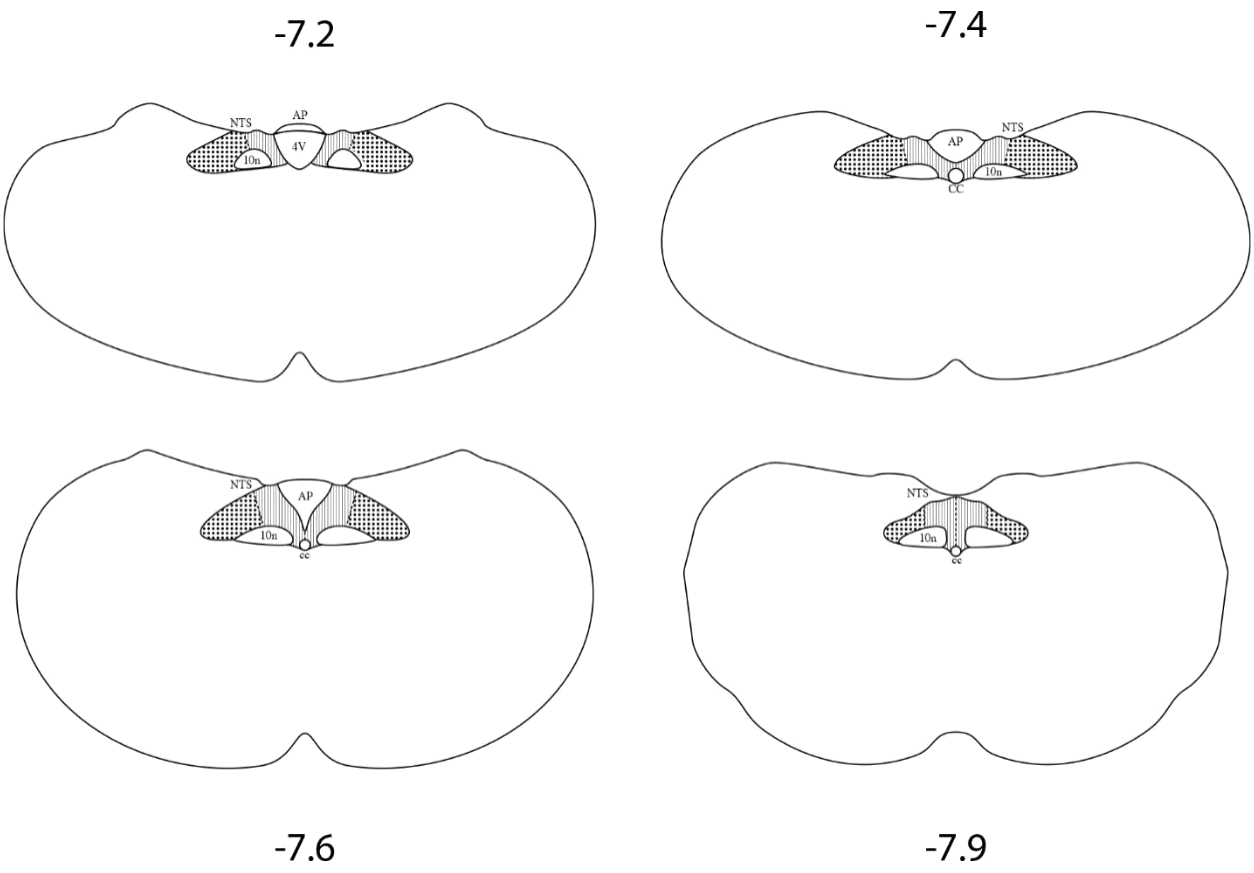

Figure 3. Schematic diagram of the relative location of the NTS and AP at 4 of the rostral-caudal levels quantified. The NTS was sub-divided into medial- and lateral- NTS. The medial NTS is denoted by the vertical patterned lines. The lateral NTS is denoted by the polka dots. (AP = area postrema, NTS = nucleus of solitary tract, 10n = dorsal motor nucleus, 4V = 4th ventricle, CC = central canal).

The AP was not subdivided at any rostral-caudal level and measured in all cross-sections in which it was present.

To quantify, confocal images were processed into two dimensional projections using Slidebook software (v.5.0, RRID:SCR_014300, Intelligent Imaging Innovations, Denver, CO). The four most in focus, sequential sections (4 um) were compressed. The images were then opened in Image J, converted to 8-bit, and inverted. The freehand selection tool was utilized to outline the medial and lateral NTS, and AP. The left and right medial and lateral NTS were measured independently; therefore, each cross-section resulted in 5 measurements. The total number of pixels 2 standard deviation from the mean were summed and then divided by the total outlined area. Two standard deviation from the mean was chosen to remove any background (Peters et al., 2014).

Microscopy

For quantification of neural processes that expressed tdTomato labeled with Cy3 fluorescence standard fluorescence microscopy at 200X magnification was utilized for quantification of all small intestinal mucosal measures and the apical/basal gland counts of the stomach mucosa, 100x was utilized for the circular-axis count half-way up the mucosal glands within the stomach (Leica DM5000 microscope; fluorescence filter cube Y3). Images of Cy3-fluorescence-stained neural processes in the medulla were scanned with an Olympus Disk Scanning Unit spinning disk confocal microscope attached to a BX61 motorized microscope (Olympus, Center Valley, PA) and an ALEXA Fluor 594 highly selective filter set at a magnification of 100X; images for illustration were set at a magnification of 200x. The confocal microscope was operated using Slidebook software (v.5.0, RRID:SCR_014300, Intelligent Imaging Innovations, Denver, CO). Image processing, including two-dimensional projections of z-series stacks of optical sections were also performed using the Slidebook software.

Photoshop software (version 6.0, RRID:SCR_014199, Adobe Systems, Mountain View, CA) was used to apply scale bars and text to figures, adjust image brightness and contrast, construct photomontages and organize the final figure layouts.

Statistics

The statistical analysis of the small intestinal mucosal has previously been described elsewhere (Serlin & Fox, 2019 – see Methods Statistics). Briefly, each small intestine and stomach measure were first averaged by section, then by animal. These averages (n = 5 mice/intestinal block or stomach region) were used to calculate the mean $\pm$ SEM for that condition. For statistical analysis of the lateral and medial NTS, the density of pixels (# of pixels/area) for the left and right side of each section were averaged. These averages (n = 7 total sections from a minimum of 5 mice/brain region) were used to calculate the mean $\pm$ SEM for that condition. Because there was just a single AP measure for each animal (n = 7/AP), the density of pixels for each AP was used to calculate the mean $\pm$ SEM for that condition. Importantly, each measurement was calculated independently of the others.

All statistical tests were performed in SPSS (IBM SPSS Statistics 23, RRID:SCR_002865) and statistical significance was set to $p < 0.05$, unless stated otherwise. Independent samples t-test were run for body weight, small intestine, stomach, and medulla morphology. A two-way analysis of variance (ANOVA) was run for all quantitative measures, with post-hoc independent samples t-tests where appropriate. All post-hoc measures were run with Bonferroni adjustments ($p < .007$ for intestine axons, terminals, crypt associated fibers, $p < .017$ for stomach total, distribution, and pattern analysis, $p < .008$ for medulla density measures). Reported interactions and post-hoc measures include all independent and dependent variables run in the analyses. Data is available on request from the authors.

RESULTS

Body Weight & Small Intestine, Stomach, and Medulla Morphology

The gastrointestinal vagal afferents are thought to transmit negative feedback signals to the central nervous system to slow and/or stop ingestive behaviors (Chambers et al., 2013; Sternson & Eiselt, 2017). Loss of vagal afferent signaling whether that be through changes in function or amount of innervation has been demonstrated to lead to alterations in food intake behavior (Schwartz et al., 1999) and body weight (Byerly & Fox, 2006; de Lartigue et al., 2014). These changes in food intake and body weight could potentially drive phenotypic (i.e. – bodyweight) and/or morphologic (i.e. – structural changes in organs) changes. To make sure any loss in innervation we observed was not due to or confounded by phenotypic or morphologic changes we quantified and compared several structural features between NT-4 KO and HET mice.

There was not a significant difference in body weight between NT-4 KO (30.03 $\pm$ 1.21 grams) and NT-4 HET (30.36 $\pm$ .68 grams) mice [$t(20) = =.23$, $p = .81$].

To investigate if there were morphological changes in the small intestine, the length of the small intestine, and the height and width of the villi were quantified. There was no difference in small intestine length between NT-4 KO ($n = 5$, 37.2 $\pm$ .72 cm) and NT-4 HET ($n = 6$, 35.7 $\pm$ .96 cm) mice [$t(9) = 1.17$, $p = .27$]. There was also no difference in villus height or width between NT-4 KO and NT-4 HET mice at any of 7 collection sites down the length of the small intestinal mucosa (Figure 4).

To investigate if there were morphological changes in the stomach, the length of the stomach containing mucosa, and the thickness of the muscle and mucosa tissue layer at each of the 4 locations around the circular axis (oral, ventral, aboral, dorsal, see methods) were quantified. NT-4 HET mice ($n = 5$, 0.92 $\pm$ .04 cm) had slightly longer stomachs than NT-4 KO mice ($n = 5$, 0.8 $\pm$ .03 cm) [$t(9) = -2.63$, $p = .03$]. The range of stomach lengths, collapsed across experimental condition, was 0.7 – 1.0 cm. In the proximal corpus, middle corpus, and antrum regions of the stomach there was no difference between NT-4 KO and NT-4 HET mice in the muscle or mucosa thickness at any of the four locations around the circular axis (Table 1).

Table 1. Mean # of Grid-Boxes ± SEM

Condition	Region	Tissue Layer							
		Muscle				Mucosa			
		Oral	Ventral	Aboral	Dorsal	Oral	Ventral	Aboral	Dorsal
HET	Prox. Corpus	2.63 ± .52	.75 ± .14	.38 ± .04	.41 ± .05	7.03 ± .69	6.02 ± .27	4.72 ± .33	5.46 ± .2
KO	Prox. Corpus	1.9 ± .12	.48 ± .06	.38 ± .04	.4 ± .07	7.57 ± .67	5.28 ± .64	3.95 ± .43	4.51 ± .48
HET	Mid. Corpus	1.97 ± .26	.99 ± .19	.34 ± .05	.6 ± .05	4.81 ± .96	4.68 ± .3	5.38 ± .46	4.51 ± .42
KO	Mid. Corpus	1.4 ± .3	.6 ± .1	.32 ± .05	.48 ± .07	4.93 ± .83	4.53 ± .25	4.42 ± .42	4.61 ± .24
HET	Antrum	1.23 ± .2	1 ± .1	.91 ± .28	.94 ± .11	2.52 ± .14	3.33 ± .24	5.35 ± .55	3.23 ± .41
KO	Antrum	.83 ± .05	.93 ± .05	.55 ± .13	.77 ± .08	2.75 ± .2	3.47 ± .24	5.83 ± .55	3.42 ± .16

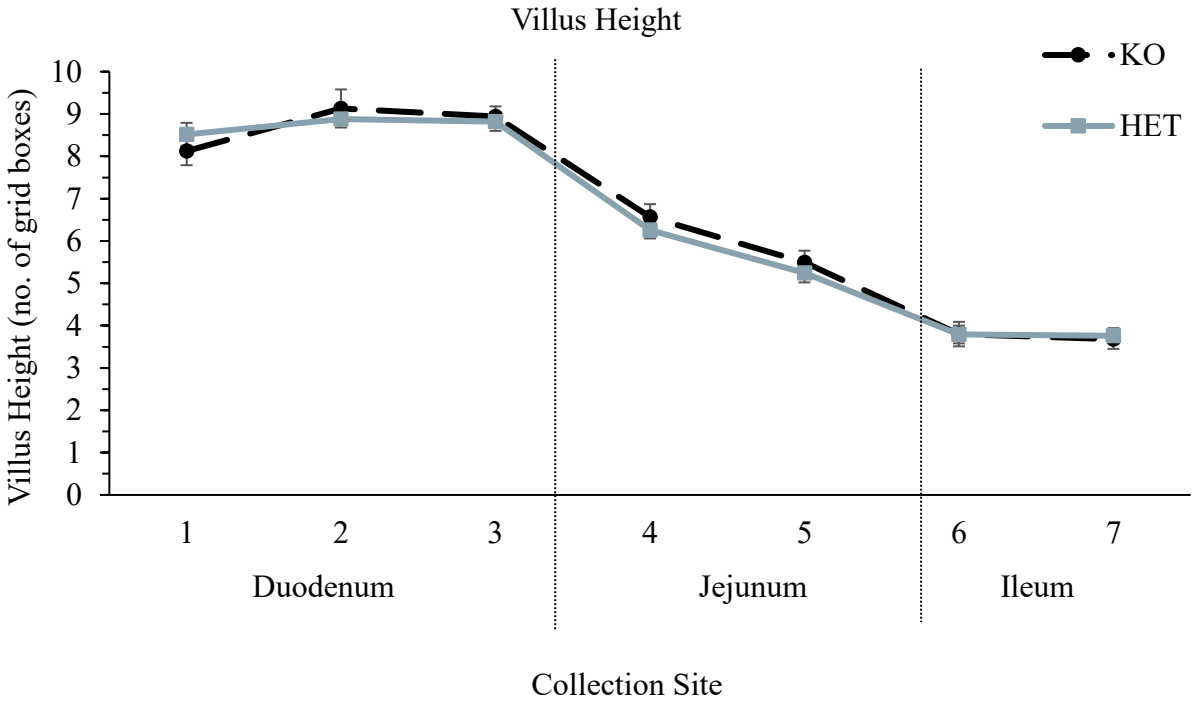

Figure 4. Quantitative comparisons of the height of villi in HET and KO mice at all 7 collection sites along the length of the entire small intestine. Data are means of each villus/section/ animal at given collection site ± SEMs (n = 5 mice/collection site). There were no significant differences indicated by a 2 x 2 mixed ANOVA between HET and KO mice ($p < .05$

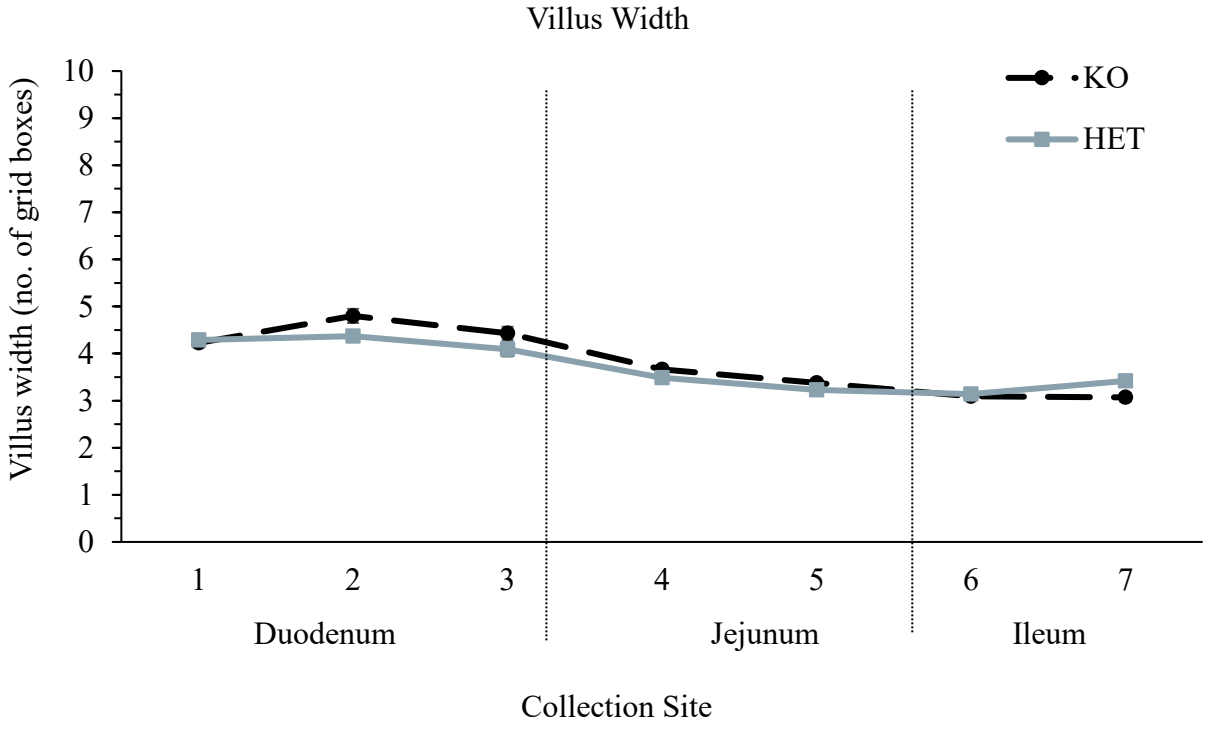

Figure 5. Quantitative comparisons of the width of villi in HET and KO mice at all 7 collection sites along the length of the entire small intestine. Data are means of each villus/section/ animal at given collection site ± SEMs (n = 5 mice/collection site). There were no significant differences indicated by a 2 x 2 mixed ANOVA between HET and KO mice ($p < .05$).

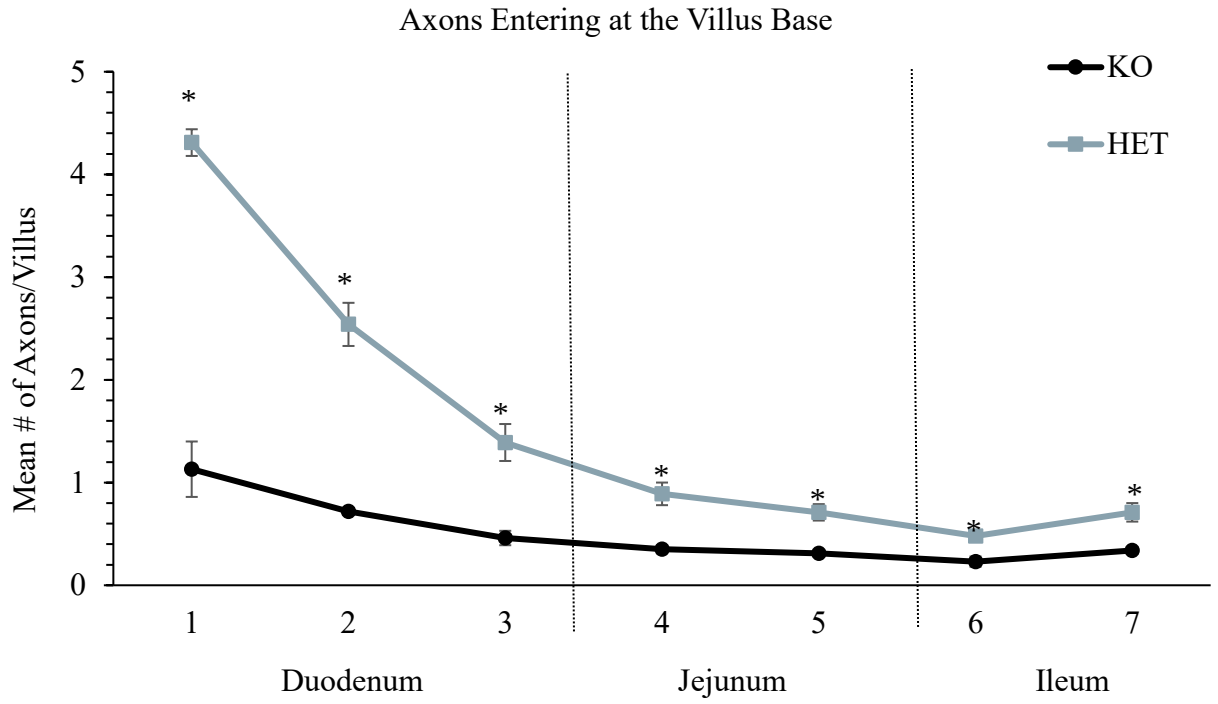

Figure 6. Quantitative comparisons of the distributions of tdTomato-labeled fibers in the mucosa of HET and KO mice at the 7 collection sites along the entire length of the small intestine. Data are means of the villi/section/animal at a given collection site. (n = 5 mice/blocks per collection site). Distribution quantified is the number of tdTomato-labeled axons entering a villus. Significant differences were indicated by a 2 x 2 mixed ANOVA with Independent t-tests post hoc tests, with Bonferroni adjustment between HET and KO groups at shared collection sites, * p < .007.

To investigate the consistency in defining the medial and lateral NTS and AP, the area quantified at each rostral-caudal level was compared between the two experimental conditions. Independent t-tests revealed there was no difference in the area quantified as the medial NTS, lateral NTS, or AP between NT-4 KO and HET mice at any rostral-caudal level (data not shown).

Although the current study did not directly investigate possible disruption to other surrounding neural networks, previous studies indicated no significant disruption in the number of myenteric neurons in the small intestine or stomach and no qualitative disruption to the dorsal motor nucleus (vagal efferents) (Fox et al., 2001). Therefore, any reduction of vagal afferents quantified in NT-4 KO mice, compared to NT-4 HET mice in the current study, is not thought to be caused by or to cause phenotypic or morphologic changes in the quantified organs.

NT-4 KO Exhibit a Dramatic Reduction of tdTomato -Labeled Innervation in the Small Intestinal Mucosa

Previously, anterograde tracing from the nodose ganglion was used to examine the projections and terminal structure of vagal afferents in the gastrointestinal tract (Berthoud and Powley, 1992; Berthoud, 1995; Powley, 2011). These foundational studies identified a single receptor type in the muscle tissue layer -intraganglionic laminar endings (IGLEs)- and two receptor types in the mucosal tissue layer – vagal crypt and vagal villus fibers – of the small intestine. Previous characterization of NT-4 KO mice revealed IGLEs were largely eliminated in the most proximal and distal regions of the small intestine compared to wildtype control mice (Fox et al., 2001). Thus, neurotrophin-4 is important for the survival of vagal afferents in the small intestine muscle tissue layer. Several quantification measures were employed to investigate if neurotropin-4 is similarly important for the survival of vagal afferents in the small intestinal mucosal layer.

Quantification of the tdtomato-labeled villus afferents revealed a significant interaction between experimental condition (KO, HET) and collection site (1-7) along the entire length of the small intestinal mucosa in the mean number of axons entering the base of a villus [$F(6, 56) = 38.91$, $p > .001$, partial nx = 81] and in the mean number of terminal brances at villus mid-height [$F(6,$ = .002]; CS4 [$t(8) = -6.99$, $p < .001$]; CS5 [$t(8) = -4.85$, $p = .001$]; CS6 [$t(8) = -2.87$, $p = .021$]; CS7 [$t(8) = -3.62$, $p = .007$] (Figure 7).

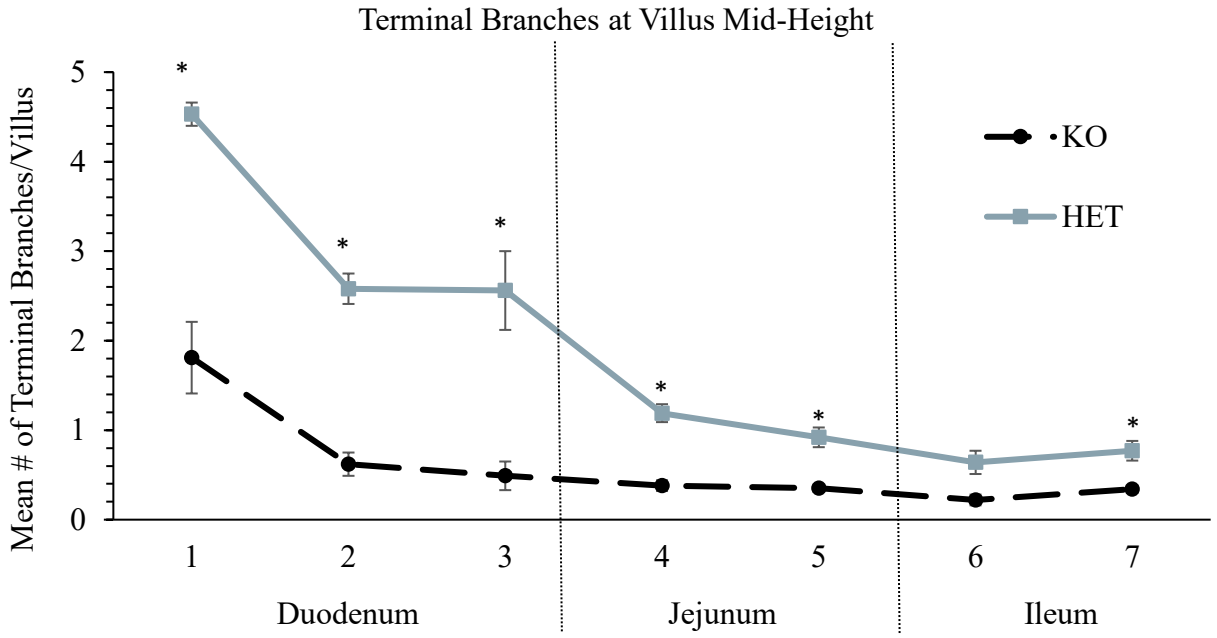

Figure 7. Quantitative comparisons of the distributions of tdTomato-labeled fibers in the mucosa of HET and KO mice at the 7 collection sites along the entire length of the small intestine. Data are means of the villi/section/animal at a given collection site. (n = 5 mice/blocks per collection site). Distribution quantified is the number of tdTomato-labeled terminal branches at villus mid-height. Significant differences were indicated by a 2 x 2 mixed ANOVA with Independent t-tests post hoc tests, with Bonferroni adjustment between HET and KO groups at shared collection sites, * $p < .007$.

Quantification of tdtomato-labeled crypt afferent associated fibers revealed no interaction between experimental condition and collection site along the length of the entire small intestinal mucosa for the mean percentage of crypts associated with fibers [$F(6, 56) = .93$, $p = .48$, $\eta 2 = .091$]. There were significant main effects of experimental condition [$F(1, 56) = 93.21$, $p < .001$, $\eta 2 = .625$] and collection site along the length of the longitudinal axis [$F(6, 56) = 48.04$, $p < .001$, $\eta 2 = .837$]. NT-4 KO mice exhibited a significant reduction in the percentage of crypts associated with fibers compared to NT-4 HET mice at a subset of collection sites (CS1 [$t(8) = -5.23$, $p = .001$], CS2 [$t(8) = -7.46$, $p < .001$], CS5 [$t(8) = -3.7$, $p = .007$]) (Figure 8).

As seen with the muscle tissue layer, current quantification of the two vagal receptor types projecting to the mucosa tissue layer of the small intestine revealed that neurotrophin-4 is important for the survival of vagal afferents in the mucosa layer too (Figure 9, 10).

NT-4 KO and NT-4 HET Mice Exhibited a Similar Distribution of tdTomato-Labeled Innervation in the Stomach Mucosa

The muscle tissue layer of the stomach has two known vagal receptor types – IGLEs and intramuscular laminar endings (IMAs) (Fox et al., 2000). Fox and others (2001) reported NT-4 KO mice exhibited no disruption to the density or distribution of IMAs or IGLEs in the stomach compared to wildtype mice. Quantification measures were employed to investigate the effects of knocking out neurotropin-4 on vagal afferents innervating the mucosa tissue layer of the stomach.

Quantification of the mean number of tdtomato-labeled fibers half-way up the stomach mucosal glands along the entire circular axis revealed an insignificant interaction between experimental condition (KO, HET) and stomach region (proximal corpus to antrum) [$F(2, 24) = .284$, $p = .755$, partial $\eta 2 = .023$]. There was no difference in the mean total number of fibers mid-way up the stomach mucosal glands at the proximal corpus (298.93 $\pm$ 18.90 fibers; 337.03 $\pm$ 26.31 fibers), middle corpus (343.93 $\pm$ 21.12 fibers; 412.5 $\pm$ 27.32 fibers) or antrum (368 $\pm$ 29.41 fibers; 395.33 $\pm$ 41.57 fibers) between NT-4 KO and NT-4 HET mice, respectively (Figure 11).

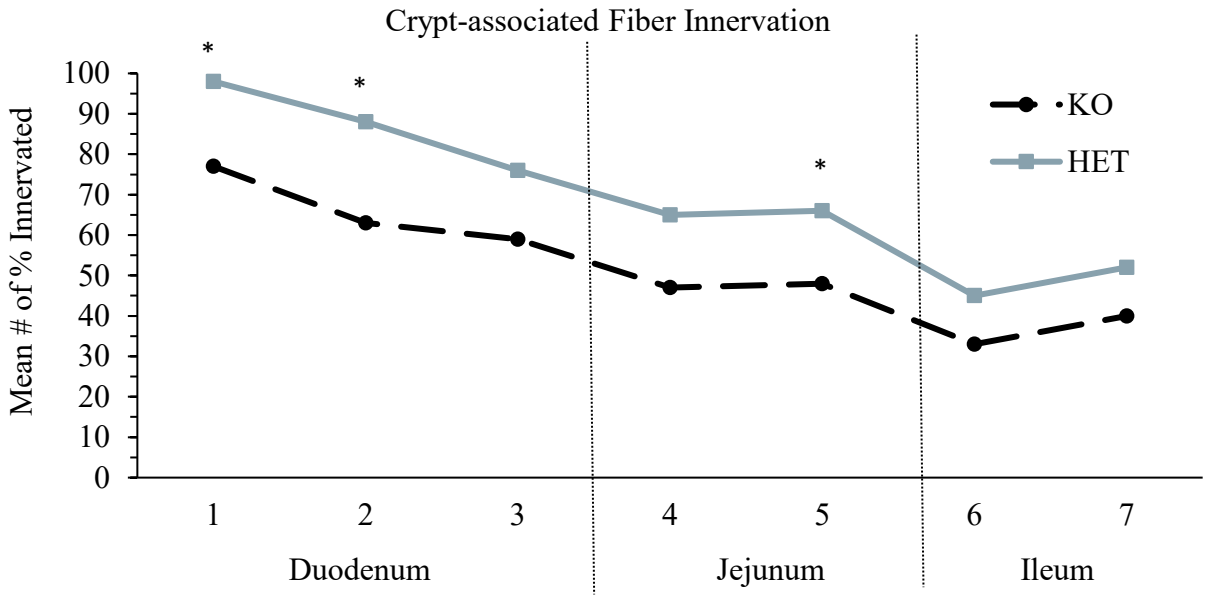

Figure 8. Quantitative comparisons of the distributions of tdTomato-labeled fibers in the mucosa of HET and KO mice at the 7 collection sites along the entire length of the small intestine. Data are means of the crypts/section/animal at a given collection site. (n = 5 mice/blocks per collection site). Distribution quantified is the percentage of crypts associated with tdTomato-labeled. Significant differences were indicated by a 2 x 2 mixed ANOVA with Independent t-tests post hoc tests, with Bonferroni adjustment between HET and KO groups at shared collection sites, * $p < .007$.

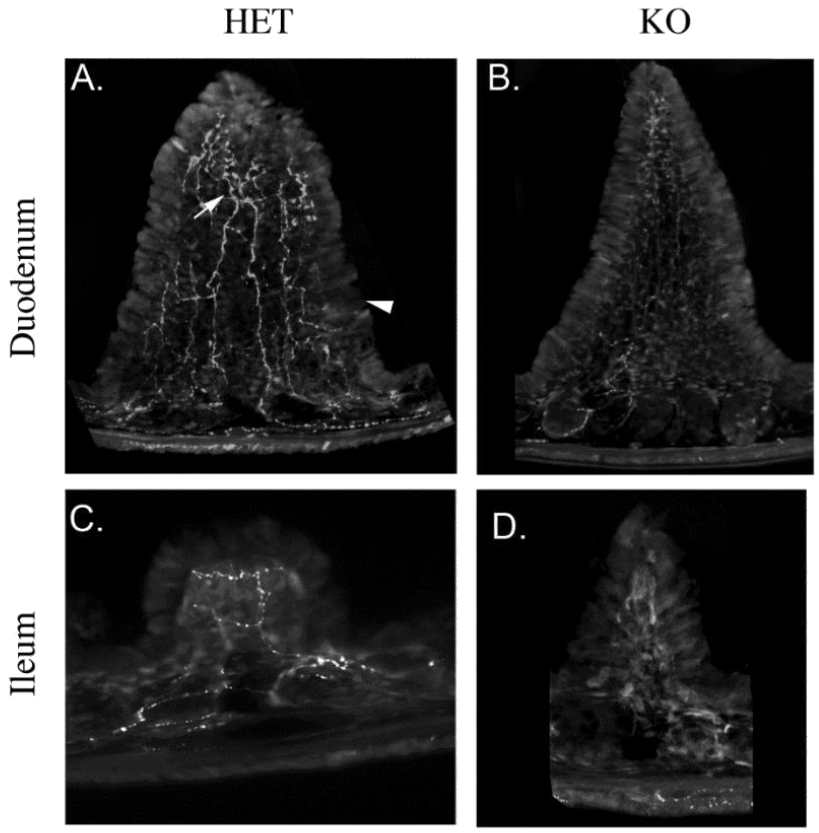

Figure 9. Examples that illustrate the organization and morphology of tdTomato-labeled fibers supplying the villi in the small intestinal mucosa. A-D. Confocal images or montages of tdTomato-labeled fibers and terminals in the duodenum (A-B) and ileum (C-D) of HET (A, C) and KO (B, D) mice. (epithelium of villus = arrowhead in A; tdtomato-labeled fiber innervating a villus = solid white arrow in A) Scale bars = ____µm.

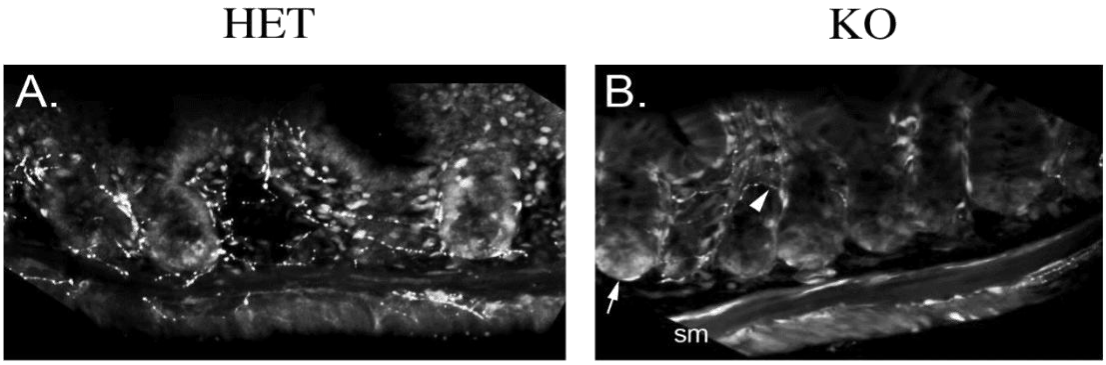

Figure 10. Examples that illustrate the organization and morphology of tdTomato-labeled crypt associated fibers in the small intestine. A-B. Confocal images or montages of tdTomato-crypt associated fibers the duodenum of HET (A) and KO (B) mice. Each of these crypts would be quantified as a "yes" but qualitatively there is a noticeable reduction in the amount of innervation per crypt. (crypt associated fiber = arrowhead in B; crypt = solid white arrow in B; sm = smooth muscle) Scale bars = ____µm.

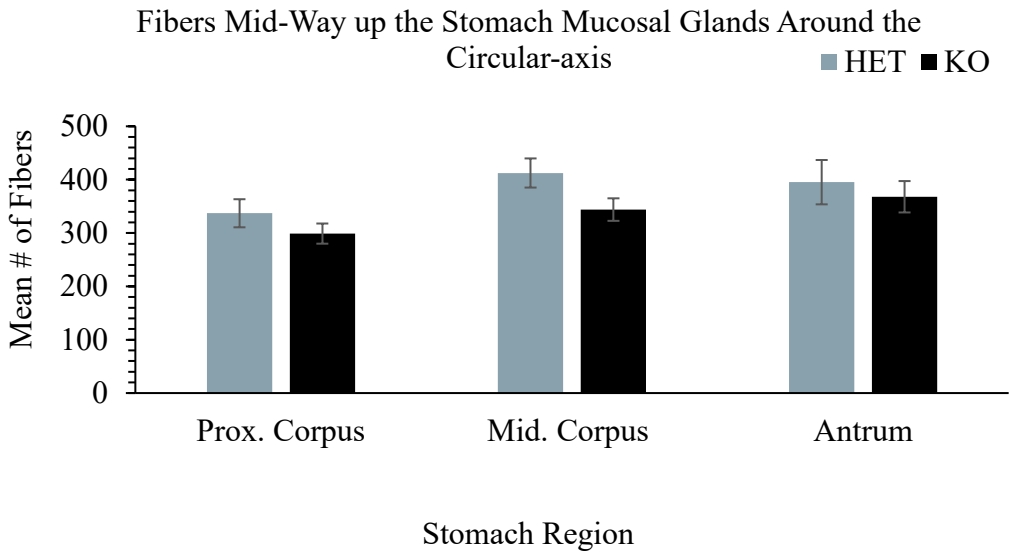

Figure 11. Quantitative comparisons of the distributions of tdTomato-labeled fibers along the circular-axis in the mucosa of HET and KO mice at the 3 regions down the length of the stomach. Data are means of the total number of fibers/section/animal at a given collection site. (*n* 5 mice/region). Distribution quantified is the mean number of tdTomato-labeled fibers mid-way up the stomach mucosal glands around the entire circular-axis. Significant differences were indicated by a 2 x 2 mixed ANOVA with Independent t-tests post hoc tests, with Bonferroni adjustment between HET and KO groups at shared collection sites, * $p < .017$.

To investigate if there was a difference in the distribution of tdtomato-labeled fibers, each cross-section was divided in half; moving clockwise, with the esophagus representing high noon, 9'oclock to 3'oclock represented the "lesser curvature" half, and 3'oclock to 9'oclock represented the "greater curvature" half (Figure 2). There was no interaction in the mean number tdtomato-labeled fibers mid-way up the stomach mucosal glands along the circular-axis half of the lesser curvature [$F(2, 24) = .143$, $p = .87$, partial $\eta 2 = .012$] or greater curvature [$F(2, 24) = .424$, $p = .66$, partial $\eta 2 = .034$]. There was no difference in the mean total number of fibers mid-way up the stomach mucosal glands along the lesser curvature half at the proximal corpus (204.27 $\pm$ 21.31 fibers; 231.63 $\pm$ 20.49 fibers), middle corpus (233.2 $\pm$ 13.32 fibers; 283.03 $\pm$ 19.71 fibers) or the antrum (205 $\pm$ 11.26 fibers; 241.9 $\pm$ 33.24 fibers) between NT-4 KO and NT-4 HET mice, respectively (Figure 12). Similarly, there was no difference in the mean total number of fibers mid-way up the stomach mucosal glands along the greater curvature half at the proximal corpus (94.67 $\pm$ 10.55 fibers; 105.4 $\pm$ 13.06 fibers), middle corpus (110.73 $\pm$ 15.02 fibers; 129.47 $\pm$ 17.21 fibers) or the antrum (163 $\pm$ 18.93 fibers; 153.43 $\pm$ 18.52 fibers), between NT-4 KO and NT-4 HET mice, respectively (Figure 13).

To investigate if there was a difference in the innervation pattern of tdtomato-labeled fibers, mucosal glands in 4 locations (12, 3, 6, 9 o'clock) along the circular axis of each cross-section were quantified for the number of fibers contacting the basal or apical third of each individua l gland (Figure 14; only select HET data shown). In the proximal corpus, there was no difference between NT-4 KO and NT-4 HET mice in the mean number of tdtomato-labeled fibers contacting the bottom [$t(8) = .4$, $p = .7$; $t(8) = .28$, $p = .78$; $t(8) = .73$, $p = .49$; $t(8) = .004$, $p = 1$] or top [$t(8) = .48$, $p = .65$; $t(8) = .2$, $p = .85$; $t(8) = -.28$, $p = .79$; $t(8) = -1.13$, $p = .29$] portion of the gland at any of the four locations, respectively. In the middle corpus, there was no difference between NT-4 KO and NT-4 HET mice in the mean number of tdtomato-labeled fibers contacting the bottom [$t(8) = -.90$, $p = .39$; $t(8) = -1.2$, $p = .27$; $t(8) = 1.04$, $p = .33$; $t(8) = -.53$, $p = .61$] or top [$t(8) = -.42$, $p = .68$; $t(8) = -1.23$, $p = .24$; $t(8) = -.73$, $p = .48$; $t(8) = -.72$, $p = .49$] portion of the gland at any of the four locations, respectively. In antrum there was no difference between NT-4 KO and NT-4 HET mice in the mean number of tdtomato-labeled fibers contacting the bottom [$t(8) = -1.65$, $p = .14$; $t(8) = .73$, $p = .49$; $t(8) = -1.61$, $p = .23$; $t(8) = -.42$, $p = .69$] or top [$t(8) = -.5$, $p = .63$; $t(8) = -1.3$, $p = .23$; $t(8) = -.58$, $p = .58$; $t(8) = -1.71$, $p = .28$] portion of the gland at any of the four locations, respectively.

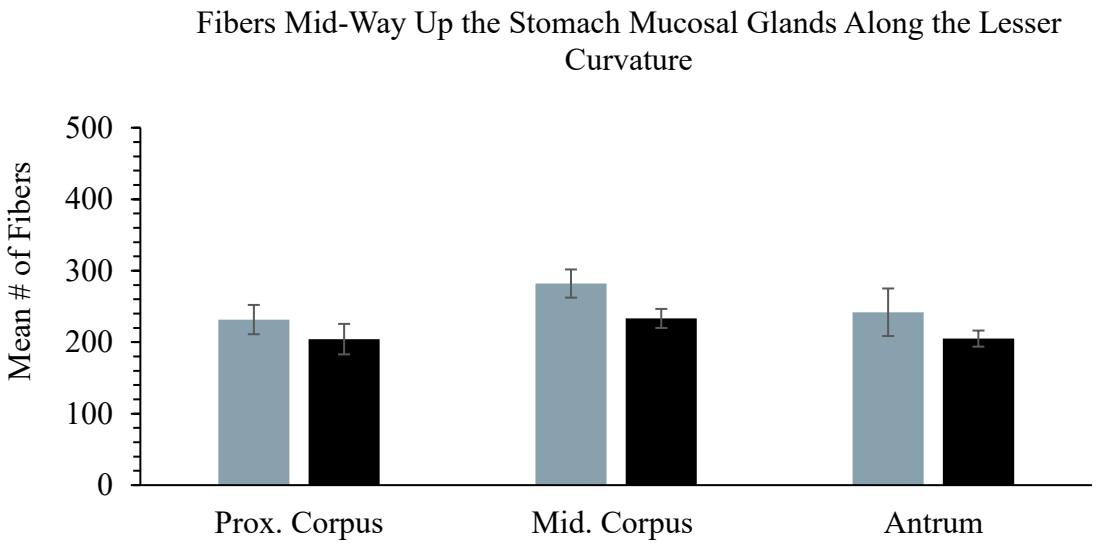

Figure 12. Quantitative comparisons of the distributions of tdTomato-labeled fibers along the circular-axis in the mucosa of HET and KO mice at the 3 regions down the length of the stomach. Data are means of the total number of fibers/section/animal at a given collection site. (*n* = 5 mice/region). Distribution quantified is the mean number of tdTomato-labeled fibers mid-way up the stomach mucosal glands around the lesser curvature half. Significant differences were indicated by a 2 x 2 mixed ANOVA with Independent t-tests post hoc tests, with Bonferroni adjustment between HET and KO groups at shared collection sites, * $p < .017$.

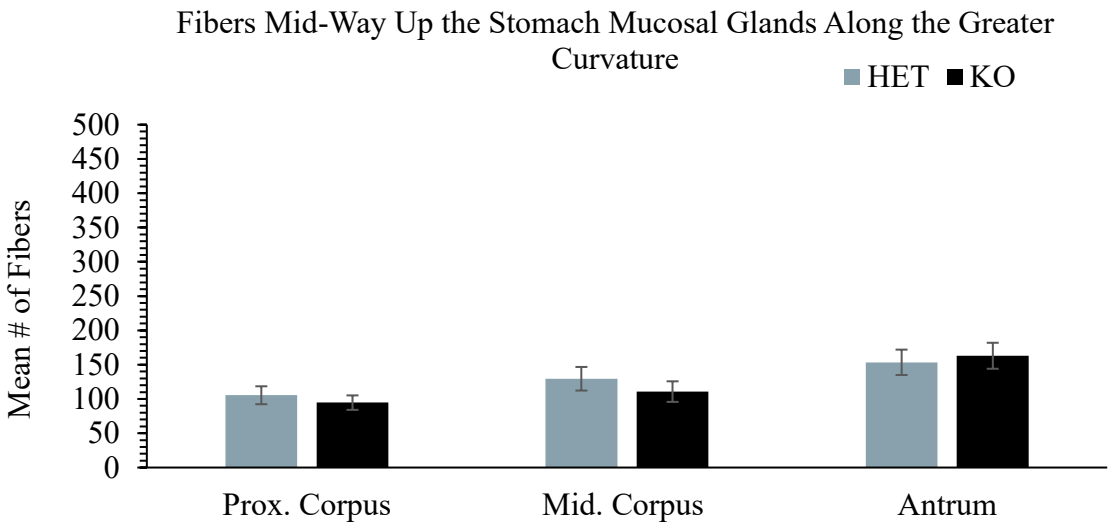

Figure 13. Quantitative comparisons of the distributions of tdTomato-labeled fibers along the circular-axis in the mucosa of HET and KO mice at the 3 regions down the length of the stomach. Data are means of the total number of fibers/section/animal at a given collection site. (*n* = 5 mice/region). Distribution quantified is the mean number of tdTomato-labeled fibers mid-way up the stomach mucosal glands around the greater curvature half. Significant differences were indicated by a 2 x 2 mixed ANOVA with Independent t-tests post hoc tests, with Bonferroni adjustment between HET and KO groups at shared collection sites, * $p < .017$.

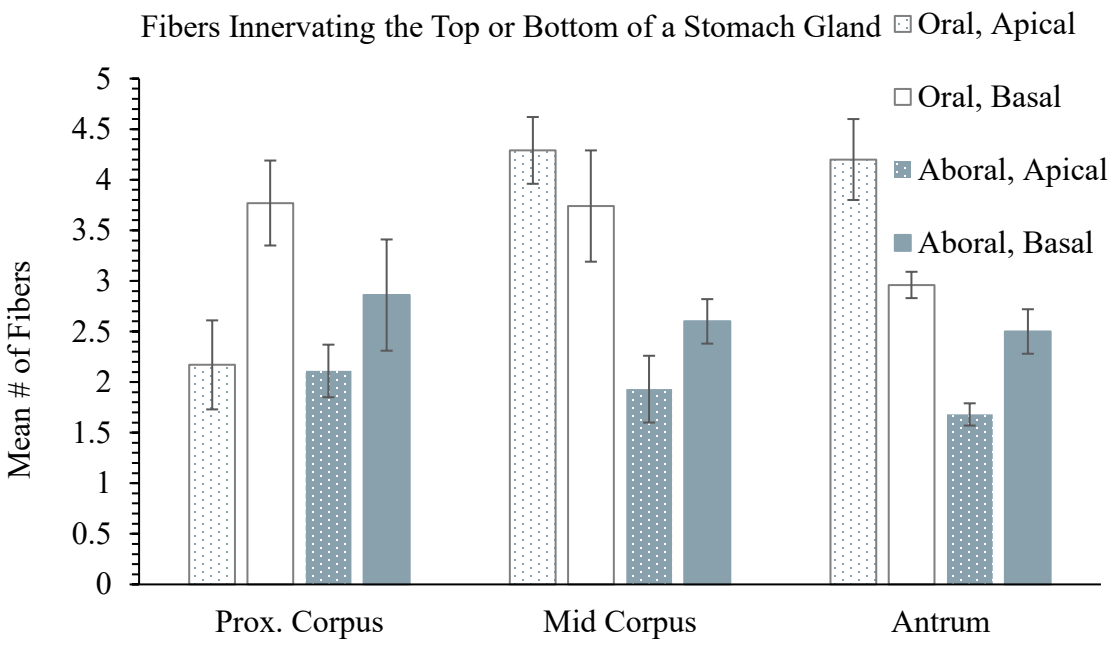

Figure 14. Quantitative comparisons of the mean number of tdTomato-labeled fibers in contact with the mucosal glands at the oral and aboral locations around the circular-axis of HET mice at the 3 regions down the length of the stomach. Data are means of the total number of fibers/section/animal at a given collection site. (n = 5 mice/region). Statistical tests were not run on HET only data.

Overall, there was no disruption to the total amount, distribution or pattern of vagal afferent innervation in the stomach mucosa in NT-4 KO mice. The survival of the mucosal fibers in the stomach, unlike those in the small intestine, appear to not be dependent on neurotrophin-4 (Figure 15).

NT-4 KO Mice Exhibit a Selective Increase in Terminal Density in the Medial NTS

The central projections of gastrointestinal vagal afferents are known to terminate along the rostral-caudal axis of the caudal-intermediate NTS and AP in the medulla (Altschuler et al., 1989; Paxinos et al., 2012). To investigate if, and if so how, the organ-specific loss observed peripherally is mirrored centrally, we quantified the density of terminal projections along the rostral-caudal axis of the medial NTS, lateral NTS, and AP.

Quantification of the density of tdtomato-labeled terminals in the medial NTS reveled no significant interaction between experimental condition (KO, HET) and rostral-caudal level (-7.2 to -7.9) [$F(5, 71) = 1.61$, $p = .34$, $\eta 2 = .076$]. There were significant main effects of experimental condition [$F(1, 71) = 74.63$, $p < .001$, $\eta 2 = .512$] and rostral-caudal level [$F(5, 71) = 45.21$, $p < .001$, $\eta 2 = .761$] in the medial NTS. NT-4 KO mice exhibited a significant increase in terminal density in the medial NTS at 4 of the rostral-caudal levels compared to NT-4 HET mice (-7.3, [$t(12) = - 3.77$, $p = .003$]; -7.4 [$t(12) = -4.82$, $p = .031$]; -7.5, [$t(12) = -d5.12$, $p < .001$]; -7.9, [$t(12) = -4.85$, $p < .001$]) (Figure 16). Both NT-4 KO and NT-4 HET mice exhibited a rostral to caudal decrease in the mean density of fibers in the medial NTS.

Quantification of the density of tdtomato-labeled terminals in the lateral NTS reveled no significant interaction between experimental condition and rostral-caudal level [$F(5, 71) = 1.74$, $p = .97$, $\eta 2 = .012$]. There was only a significant main effect of rostral-caudal level [$F(5, 71) = 4.5$, $p = .001$, $\eta 2 = .241$] in the lateral NTS. Both NT-4 KO and HET mice exhibited a rostral to caudal decrease in the mean density of fibers in the lateral NTS (Figure 17).

Quantification of the density of tdTomato-labeled terminals in the AP reveled no significant interaction between experimental condition and rostral-caudal level (-7.3 - -7.6) [$F(4, 59) = .264$, $p = .90$, $\eta 2 = .018$] (Figure 18). There was a trend towards a significant main effect of experimental condition [$F(1, 59) = 4.16$, $p = .05$, $\eta 2 = .066$]. There was an insignificant main effect of rostral-caudal level [$F(4, 59) = 1.35$, $p = .26$, $\eta 2 = .084$].

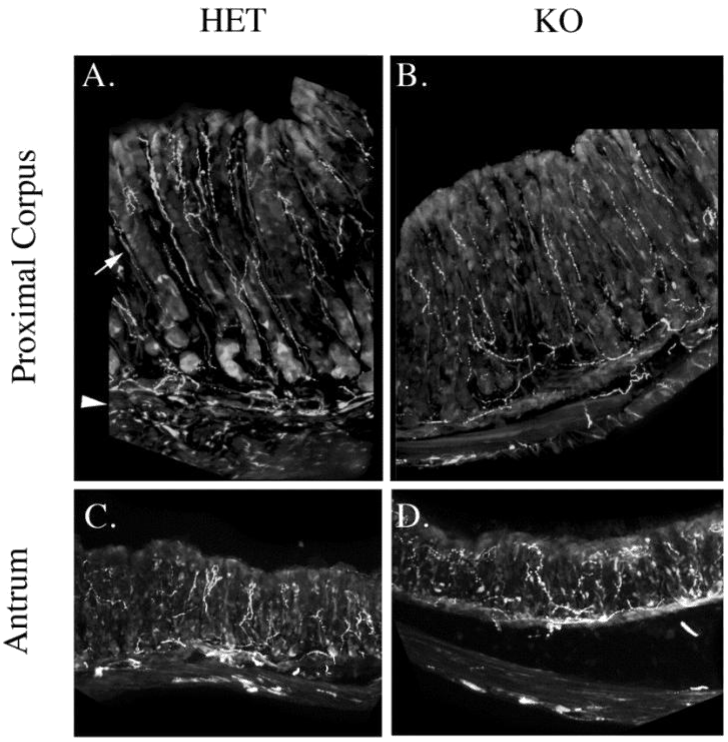

Figure 15. Examples that illustrate the organization and morphology of tdTomato-labeled fibers supplying the mucosa in stomach. A-D. Confocal images or montages of tdTomato-labeled fibers and terminals in the proximal corpus (A-B) and antrum (C-D) of HET (A, C) and KO (B, D) mice. (smooth muscle = arrowhead in A; stomach mucosal gland with label = solid white arrow in A) Scale bars = ____µm.

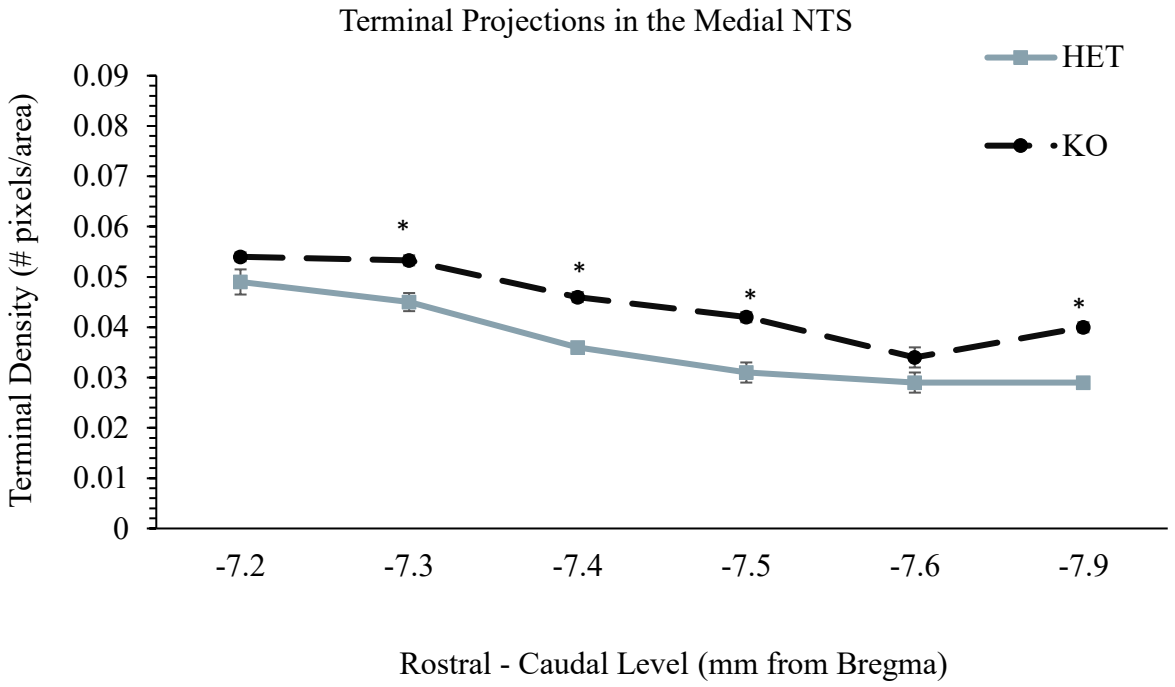

Figure 16. Quantitative comparisons of the distributions of tdTomato-labeled fibers in the medial NTS of HET and KO mice at the 6 rostral-caudal levels spanning the NTS. Data are means of the terminal density/section/animal at a given collection site. (n = 7 sections/level). Distributions quantified included the number of tdTomato-labeled axons terminating within the medial NTS. Significant differences were indicated by a 2 x 2 mixed ANOVA with Tukey's post hoc tests between KO and HET groups at shared collection sites, * $p < .008$.

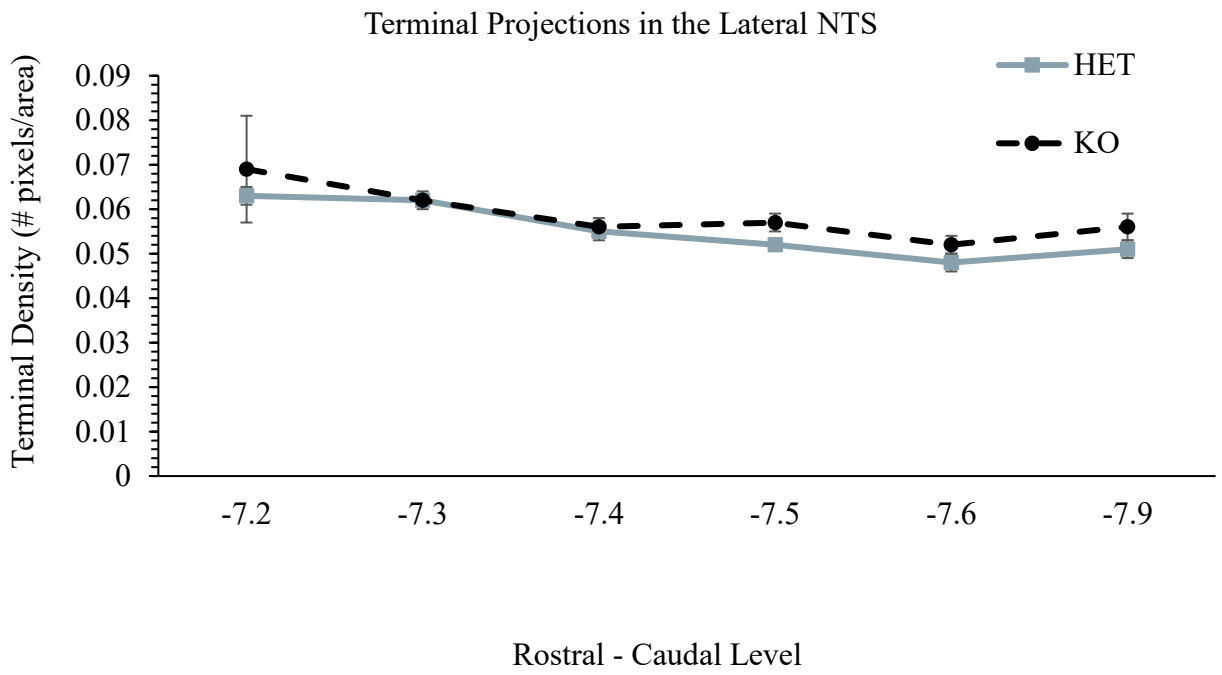

Figure 17. Quantitative comparisons of the distributions of tdTomato-labeled fibers in the lateral NTS of HET and KO mice at the 6 rostral-caudal levels spanning the NTS. Data are means of the terminal density/section/animal at a given collection site. (n = 7 sections/level). Distributions quantified included the number of tdTomato-labeled axons terminating within the lateral NTS. There were no significant differences as indicated by a 2 x 2 mixed ANOVA, * $p < .008$.

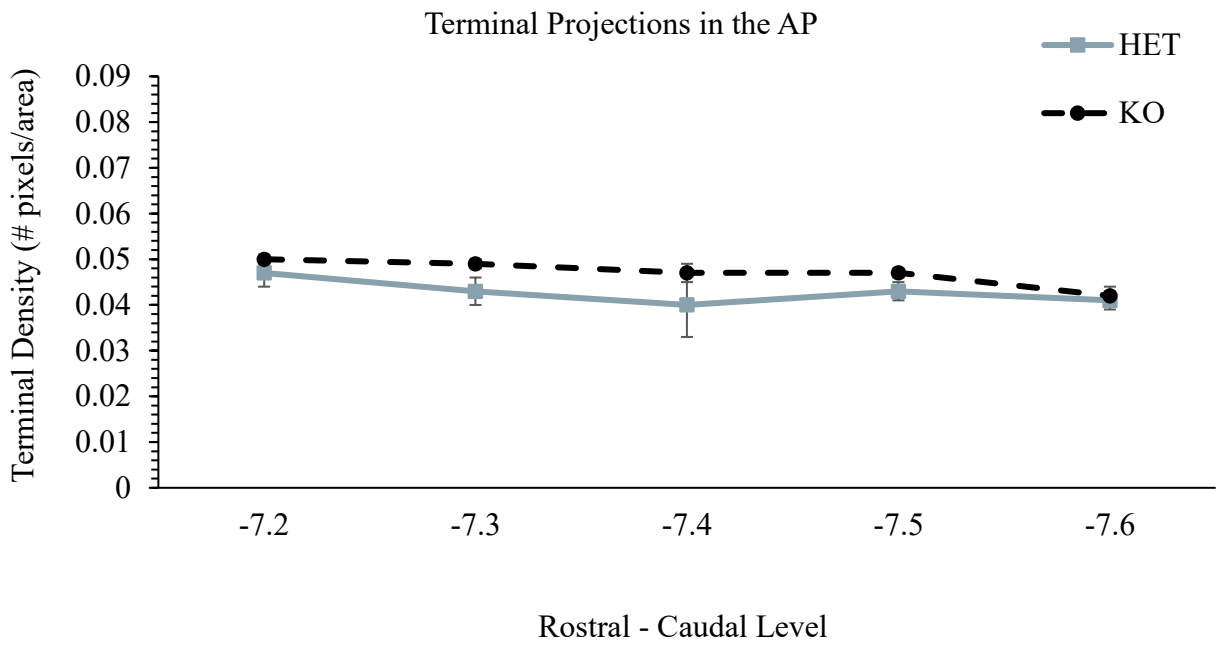

Figure 18. Quantitative comparisons of the distributions of tdTomato-labeled fibers in the AP of HET and KO mice at the 5 rostral-caudal levels. Data are means of the terminal density/section/animal at a given collection site. (n = 7 sections/level). Distributions quantified included the number of tdTomato-labeled axons terminating within the AP. There were no significant differences as indicated by a 2 x 2 mixed ANOVA, * $p < .008$.

Exploring the organization of the central projections of vagal afferents of NT-4 KO and HET mice revealed an area specific increase in the medial NTS, only (Figure 19).

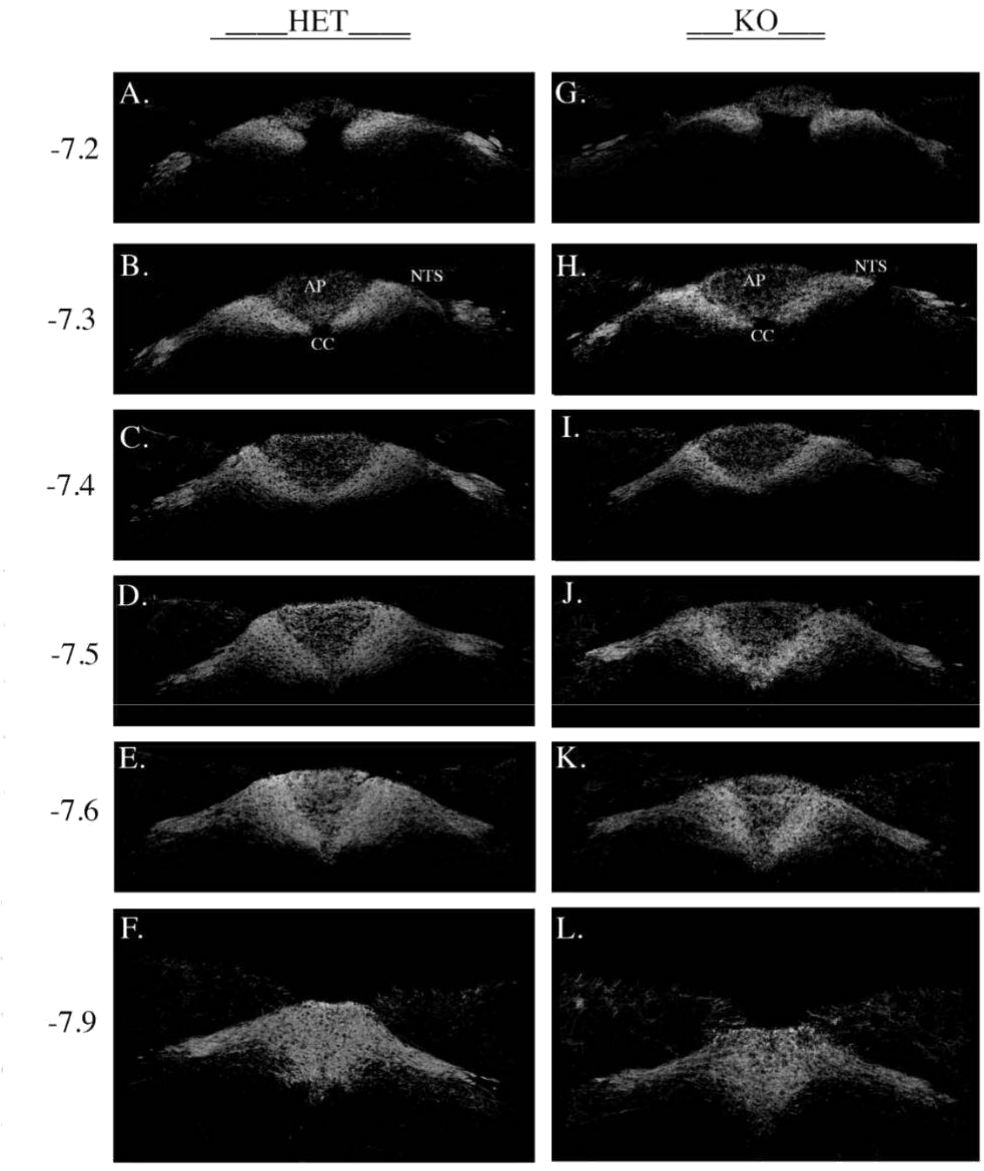

Figure 19. Examples that illustrate the density and organization of tdTomato-labeled terminals projecting to the medial and lateral NTS and AP of HET and KO mice. A-G. Confocal images or montages of tdTomato-labeled axonal terminals in HET (A-F) and KO (G-L) mice. Numbers on the left indicate rostral-caudal coordinates from Bregma (mm). (AP = area postrema, NTS = nucleus of solitary tract, CC = central canal) Scale bars = ____μm.

DISCUSSION

There is a gap in our understanding about the relationship between peripheral and central vagal afferent axonal projections. Investigating their structural relationship and topographic organization can provide important clues into "how" and "what" information from the peripheral organs is disseminated or converged centrally, and how this communication is altered in diseased states like obesity. Overall, the results of the present study revealed that in the periphery NT-4 KO mice exhibit a significant elimination of mucosal vagal afferents in the small intestine, but not in the stomach. Furthermore, centrally NT-4 KO mice exhibit an increase in vagal terminal projections along a portion of the rostral-caudal axis in the medial NTS.

Small Intestine and Stomach

Our current findings corroborate previous hypotheses that the loss of peripheral vagal afferents in NT-4 deficient mice is organ-specific. Original characterization of NT-4 KO mice reported a 90 and 81% reduction of muscular vagal afferent innervation in the duodenum and ileum, respectively, and observed no significant loss of muscular vagal afferents in the stomach (Fox et al., 2001). Similarly, we quantified a 75 and 55% reduction in vagal villus afferents in the duodenum and ileum, respectively, a 22% reduction in vagal crypt-associated afferents, and no significant loss of mucosal vagal afferents in the stomach.

The slight discrepancy in percent loss between ours and the previous characterization of vagal muscle afferents could be a function of the different labeling techniques used and/or the background of the mouse models utilized. In the present study, we utilized a transgenic mouse model that fluorescently labels the majority of nodose ganglion neurons and their neuronal components (i.e. – axons, dendrites, and terminals) (Stirling et al., 2005; Gautron et al., 2011). Gautron and others (2011) characterization of the Nav1.8-Cre-tdTomato mouse model suggested that the small subset of nodose ganglion neurons not fluorescently labeled most likely project to the gastrointestinal tract. Therefore, the vagal mucosal loss observed in our NT-4;Nav1.8-Cre-tdTomato mouse model may be as great as the vagal muscle loss Fox and others (2001) observed using WGA-HRP, the entire loss may just not be visible with our chosen labeling method.

The discrepancy in percent loss between our and the previous characterization could also possibly be due to a difference in genetic background. The neurotropin-4 knockout mice used in the original characterization were on a S129, while ours were on a C57BL6. (The whole mount tissue is and has been ready to quantify. Due to the pandemic I have been unable to go to lab to quantify IGLEs between KO and HET mice to see if the difference is similar to what was observed between KO and control mice on the S129 background. I can confidently say that qualitatively it appeared that NT-4 KO mice did exhibit a significant loss of IGLEs, suggesting that the difference in genetic background was not a factor.)

It is known that as well as labeling the majority of nodose ganglion neurons, the Nav1.8-Cre-tdTomato mouse model also labels a small percentage of gastrointestinal projecting dorsal root ganglion neurons (Gautron et al., 2011; Serlin & Fox, 2019). Interestingly though, genetically knocking out neurotrophin-4 was as efficient in eliminating the vagal mucosal innervation in the small intestine as surgically eliminating (bilateral subdiaphragmatic vagotomy) the gastrointestinal vagal afferents (Serlin and Fox, 2019). The similar density and distribution of fiber loss between the genetic and surgical technique suggests that the surviving tdtomato-labeled fibers in NT-4 KO mice are most likely of spinal origin, and not surviving vagal fibers.

Bilateral subdiaphragmatic vagotomized mice did exhibit a greater loss of mucosal vagal afferents in the most proximal duodenum (Block 1) than NT-4 KO mice, each compared to their controls respectively (compare Figure 4a, b in Serlin & Fox, 2019 to Figure 6, 7). The greater amount of remaining vagal afferent innervation in the proximal duodenum of NT-4 KO mice could be due to a passive or an active "rescuing" effect by the neurotrophin(s) supporting the vagal afferent innervation within the stomach. Our current findings corroborate previous findings that neurotrophin-4 is not sufficient or necessary for the survival, differentiation, or growth of nodose ganglion neurons projecting to the stomach. It is arguable, given the undeniable importance of gastric signals in the homeostatic regulation of ingestion and digestion (Phillips & Powley, 1996), that multiple neurotrophins support the survival, development, and maintenance of gastric vagal afferents as a protective measure. The transition-zone between "gastric" and "small intestine" growth factors may be overlap enough that there was passive rescuing by gastric growth factors into the duodenal bulb supporting the survival of some intestinal vagal afferents and/or differentiation of gastric vagal fibers into intestinal vagal fibers.

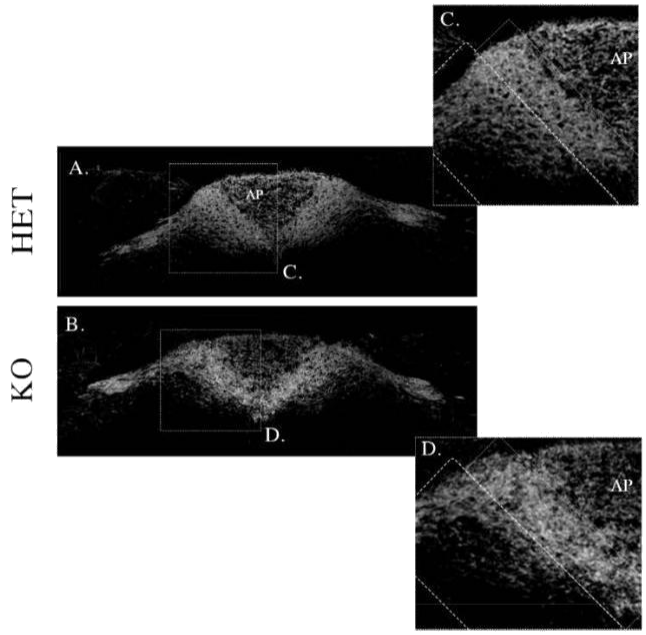

Figure 20. Example that illustrates the mediolateral density and organization of tdTomato-labeled terminals projecting in the medial- and lateral- sub-region of the medial NTS of HET and KO mice. A,B. Confocal images or montages of tdTomato-labeled axonal terminals in HET (A) and KO (B) mice at -7.5 anterior-posterior from Bregma. C, D. KO mice exhibited a qualitative increased terminal density in the medial sub-region (inner box bordering the AP) and reduced terminal density in the lateral sub-region (outer box with thicker dotted lines) (D) compared to HET mice (C). (AP = area postrema) Scale bars = ____µm.

Alternatively, it is possible that a subset of the vagal afferents innervating the most proximal duodenum may similarly be supported by multiple neurotrophins as a protective measure. Vagal afferents innervating the duodenal bulb are arguably as important as the gastric signals in the homeostatic regulation of ingestion and digestion (Bai et al., 2019; Berthoud et al., 1997; Emond et al., 2001; van de Wall et al., 2005). Emond and others (2001) demonstrated an additive effect of c-fos expression when gastric loading and infusion of duodenal nutrients occurred simultaneously, rather than independently. Bai and others (2019) have also suggested, optogenetically, that the vagal afferents in the muscle layer of the small intestine play a pivotal role in signaling satiation. Given their importance and prime location at one of the earliest sites of the body's contact with food, gut bacteria, and immunogens (Bonaz et al., 2017; Cawthon & de La Serre, 2018; Chapman et al., 1999; Holzer, 2007) an active rescuing of mucosal fibers in the duodenal bulb may have occurred. Because NT-4 KO mice do not differ from their wildtype controls in overall bodyweight or total daily/weekly food intake (Fox et al., 2001), investigating the function of these surviving fibers could provide important clues about which signals from the small intestine are pivotal for satiation. We think it is possible the surviving fibers are involved in a local reflexive loop regulating gastric dumping into the small intestine.

Ingestion of a meal triggers a dynamic process of gastric relaxation and contraction to accommodate, breakdown, and push ingested contents along the GI tract (Janssen et al., 2011). There are many mechanisms regulating and modulating this dynamic process of gastric tone (Azpiroz, 1994). One mechanism that mediates gastric tone is the sensing of nutrient load in the small intestine via the vagus nerve (Azpiroz, 1994). It has been demonstrated that disruption of this vagal intestinal feedback loop underlies subtypes of gastroparesis (Lin, 1994). Future studies should investigate the transit time of an ingested meal between NT-4 KO and wildtype mice. The findings may have important insights into the synergism between the stomach and small intestine in regulating GI motility.

Little is know about the density and distribution pattern of gastric vagal mucosal afferents. While the aim of the current study was to investigate if there was a difference in the amount of innervation between the two experimental conditions, the quantification approach used provided a crude map of the innervation patterning of the vagal afferents within the gastric mucosa. Traveling down the corpus mucosa towards the pylorus, there was a slight increase in the amount of total vagal innervation. As a whole, the lesser curvature of the stomach mucosa had a greater

amount of innervation than the greater curvature. Interestingly, the disparity in the amount of innervation between the lesser and greater curvature halves lessened traveling distally towards the small intestine.

The significance of this vagal pattern of innervation remains unknown. Interestingly, we previously demonstrated the vagal afferent mucosal innervation in the small intestine exhibits the opposite patterning with a more even distribution around circular-axis in the more proximal than distal half (Serlin & Fox, 2020). The relatively even distribution of vagal mucosal innervation along the circular-axis in select regions of the stomach and small intestine may signify 1) intra-organ regional differences in function and 2) importance of the select region with even distribution as this patterning optimizes sensing of luminal contents.

We did observe a difference in stomach size between NT-4 KO and HET mice. This was most likely a floor effect. Regardless, we standardized the harvesting of the stomach regions quantified to consistently measure the same region from animal to animal.

Medulla Oblongata – Dorsal Vagal Complex

NT-4 knockout mice are born without over half of their nodose ganglion cell bodies. The loss of the cell bodies results in a loss of both the central and peripheral projections of those would-be neurons. The loss centrally was depicted in a seemingly codified manner. There was no difference in the density of vagal projections within the lateral NTS or AP along the rostral-caudal axis between NT-4 KO and HET mice. There was an increase in the density of vagal afferent projections along the rostral-caudal axis within the medial NTS of NT-4 KO mice. In addition, further qualitative inspection revealed a consistent increase-decrease patterning of terminal density mediolaterally within the medial NTS (Figure 3, 19).

In the medial NTS, there was no difference in terminal density between the two experimental conditions in the most rostrally quantified level (-7.2). At this more rostral level the gelatinous nucleus (SolG) starts to become more prominent. The gelatinous sub-nucleus in the NTS is thought to receive input from the stomach (Paxinos et al., 2012; Altschuler et al., 1991; Gwyn et al., 1985; Shapiro and Miselis, 1985). We did not see any significant difference in peripheral afferent terminals within the stomach between experimental conditions. On the other hand, counterintuitive to what we expected given the >70% loss of vagal terminals in the small intestine, NT-4 KO mice exhibited an increase in terminal density in the medial NTS at all but one

of the remaining rostral-caudal levels quantified (-7.3 to -7.5, -7.9). While we expected to see an overall reduction in central terminals, an increase makes evolutionary sense.

The ingestion of nutrients is a basic human survival need, and therefore, arguably, is a highly conserved behavior. It makes sense that the "feeding" circuits can and do engage in large-scale neuroplastic remapping to protect and promote energy homeostasis. Vaughn and others (2017) observed vagal terminal remodeling in the NTS following 7 and 21 days of exposure to a high-energy dense (HF) diet. After 7 days on a HF diet, rats, exhibited a significant decrease in terminal density in the NTS compared to controls on a low-energy dense diet. But, after 21 days on a HF diet they observed a significant increase in terminal density in the NTS compared to the controls. This observed upregulation is similarly counterintuitive given that increased weight gain and obesity are hypothesized to trigger (or be triggered by) a reduction or decreased sensitivity in receptor prevalence or neural innervation in the periphery (de Lartigue, 2016). In our lab, we have observed an upregulation in trkB-labeled terminal density in the ipsilateral NTS following a unilateral supernodose vagotomy (Gilland and Fox, data not published).

This neuroplastic remapping, following an insult or challenge, highlights the importance of the gastrointestinal neurofeedback in regulating energy homeostasis and the dynamic relationship between the peripheral and central vagal axonal terminal projections. Qualitative investigation into the terminal density patterning within the medial NTS suggested, that while there was an overall increased density in the medial NTS, this increase may have been due to an up-and-down regulation of subsets of central terminals within the medial NTS.

Overall, it appeared that the increase in the medial NTS was largely due to an increase in the more medial-half of the medial NTS (Figure 19, 20). NT-4 KO mice appeared to exhibit a greater density along the AP-NTS boundary (commissural) compared to HET mice. This necklace-like boundary includes the solitary commissural (SolC), the subpostrema area (SubP), and more rostrally the SolG sub-nuclei. All of these sub-nuclei play a role in regulating food intake through gastrointestinal feedback via vagal projections primarily terminating within the stomach (Gwyn et al., 1985; Fodor, 2007; Pirnik et al., 2011; Altschuler et al., 1991). Interestingly, this necklace-like increase is a similar to the pattern of increase depicted in Vaughn and others' (2017) rats following 21 days on a HF diet (see their Figure 5). What makes this interesting is while the NT-4 KO mice do not differ from their wildtype controls in body weight on a HFD (Byerly & Fox, 2006), the rats in Vaughn and others have an increase in bodyweight. Despite the similar plasticity of patterning

in the NTS one group appeared to be buffered from the weight gain. The difference may be due to a difference in species, but further investigations into the protective compensatory mechanisms in NT-4 KO mice may lead to insights about differences impacts of obesity throughout development and potential treatments.

Traveling outward from the necklace-like shape, within the boundaries of the medial NTS, NT-4 KO mice qualitatively appeared to exhibit a decrease in terminal density compared to HET mice (Figure 19, 20). More specifically, NT-4 KO mice exhibited a qualitative decrease in the solitary nucleus dorsal lateral (SolDL), central (SolCE), medial (SolM), and intermediate (SolIM) sub-nuclei of the NTS. These more lateral sub-nuclei within the medial NTS send projections to the central lateral and lateral parabrachial nucleus (Herbert et al., 1990). The parabrachial nucleus serves as a relay station of gastrointestinal information, that arises from vagal afferent projections onto second-order neurons in the NTS, to the forebrain (Roman et al., 2016). Disruption to the transmission of information to the parabrachial can lead to severe alterations in food intake and body weight (Palmiter, 2018). As far as we know, it remains unclear the origin of the gastrointestinal afferent input terminating within these more lateral sub-nuclei. Our data suggests the origin may be small intestinal vagal afferents, but more detailed investigation is necessary to be conclusive.

The functional significance and meaning of this medio-lateral increase and decrease in the medial NTS remains to be determined. Genetic deconstruction and functional coding of the gastrointestinal vagal afferent projections within the NTS suggested that more medially (necklace-like shape) terminating projections are involved in nutrient detection and more laterally terminating projections are involved in detecting gastrointestinal stretch (Williams et al., 2016); suggestive of a mediolateral topographic relationship organized by function. Genetic mapping of peripheral and central vagal terminals of different transgenic mouse models indicated a medio-lateral stomach, intestine NTS organizational pattern (Bai et al., 2019, compare Figure4, S4); suggestive of a mediolateral topographic relationship organized by organ. Neuronal c-fos expression within the NTS following gastric distention (Willing & Berthoud, 1997; Fraser et al., 1995), duodenal nutrient infusion (Phifer & Berthoud, 1998; Zittel et al., 1994), and ingestin of a meal (Emond & Weingarten, 1994; Rinaman et al., 1998). Do similarly suggest the central disseminatin of different peripheral gastrointestinal stimuli. But, regardless of the stimulus, a more lateral NTS c-fos pattern was exhibited. The current lack of congruence about the mediolateral

organizational pattern of the dissemination of gastrointestinal information in the NTS could be due to a lack of adequate and appropriate stimuli to investigate. Therefore, to understand the functional meaning of the terminal density we observed, further investigation into the distinct and shared signals communicated by the vagal afferents innervating the stomach and those innervating the small intestine that regulate energy homeostasis must be further investigated. Few studies have actually investigated these organ-specific functional contributions and the ones that have, have largely reported opposing findings (Deutsch & Gonzalez, 1980; Phillips & Powley, 1996; Young & Deutsch, 1981). Furthermore, the techniques utilized in these previous studies caused large disruptions to physiology and the vagal networks being investigated, bringing into question the physiological significance of the feeding behavior being measured.

The most common working theory is that the vagal afferents innervating the stomach are involved in detecting and signaling the volume of food consumed, and the vagal afferents innervating the small intestine are involved in detecting and signaling the chemical composition of the food, and that both are post-ingestive cues satiety cues (Powley & Phillips, 2004; Liebling et al., 1975; Rauhofer, E.A., et al., 1993). Several anatomical, electrophysiological, and behavioral studies, selectively investigating the stomach, support that the vagal afferents innervating the stomach do play a role in volume detection (Powley et al., 2011; Berthoud et al., 2001; Phillips & Powley 1996; Zagorodnyuk et al., 2003; Zagorodnyuk et al. 2001; Rodrigo et al., 1975; Berthoud and Powley, 1992; Berthoud and Neuhuber, 1994; Berthoud et al., 1997; Fox et al., 2000). Importantly though, only the gastric muscle vagal neural network was investigated in these previous studies. Previous studies have demonstrated that vagal afferents are also observed to densely innervate and terminate in the mucosal tissue layer of the stomach (Berthoud et al., 2001; Serlin & Fox, 2019). It seems reasonable to hypothesize there would be specialized endings in the mucosa tissue layer in the stomach involved in functions other than volume detection, given their proximity to one of the earliest sites of the body's contact with food, bacteria, and immunogens. Therefore, it is conceivable that the stomach may also be involved in detection of the chemical composition of luminal contents as previously suggested by Deutsch & Gonzalez, 1980.

Several anatomical, electrophysiological, and behavioral studies, selectively investigating the small intestine, support that the vagal afferents innervating the small intestine do play a role in macronutrient detection (Liebling et al., 1975; Phifer & Berthoud, 1998; Chi et al., 2007). But, it

has also been demonstrated that the small intestine detects distention (i.e. – volume) that contributes to the cessation of a meal (Hirst et al., 1975; Williams et al., 2016; Bai et al., 2019).

Therefore, the question of whether gastric distention and macronutrient detection are two separate, distinct, and organ-monopolized post-ingestive mechanisms inhibiting food intake still remains. Based on previous behavioral data revealing NT-4 KO mice exhibit decreased sensitivity to meal-associated lipid feedback (Chi & Powley, 2007), hyperphagia of an energy-dense diet (Byerly & Fox, 2006), alterations in meal patterns (Fox et al., 2001), and no overall difference in bodyweight or total daily/weekly food intake from their wildtype controls, we think the increase of terminal density in the medial NTS we quantified in NT-4 KO mice, may be neuroplastic compensation to maintain energy homeostasis. Whether this compensation is an enhancement of known or unknown gastric functions, similar to the heightened remaining senses observed in someone who is blind or deaf, or a gain-of-function remains to be determined.

It is important to note, our mouse model does not selectively label gastrointestinal vagal afferents and neurotrophin-4 does play a supportive role in other neuronal populations. Despite this, we think it is unlikely that the reduction of central terminal projections in the medial NTS is due to a disruption of vagal innervation to other peripheral organs. The other known central projections of vagally innervated peripheral organs - the heart and respiratory system terminate more in the area of the lateral NTS (Corbett et al., 2005; McGovern et al., 2014), where we saw no difference in terminal density between NT-4 KO and HET mice.

NT-4 KO and HET mice exhibited no difference in AP terminal density. Despite the visible rostral-caudal increase in the size of the AP, there was not a main effect of level, indicating the density of terminal projections remained stable in the AP along the rostral-caudal axis. This highlights the important functions of the AP and may provide clues as to why the qualitative increase in the medial NTS was along the AP boundary.

Limitations

Neurotrophin-4 is a nerve growth factor involved in the regulation of neuronal survival, differentiation, and growth during development and throughout life. This growth factor appears to be involved in rescuing neurons during the first wave of cell death during development (Patel & Krimm, 2012). In the mouse model utilized in this study, the nerve growth factor

neurotrophin-4 was globally knocked out at conception. Knocking out both NT-4 alleles was not life threatening, and mice appear similar to controls in growth, longevity, and mobility, and are capable of producing viable offspring (Conover et al., 1995; Erickson et al., 1996). NT-4 KO (Fox et al., 2001, Byerly & Fox, 2006, Chi & Powley, 2007) and knock-in (Chi et al., 2004) mice do exhibit alterations in meal pattern parameters, but interestingly, neither knock-out nor knock-in mice differed from their wildtype controls in overall bodyweight or total daily/weekly food intake. This suggests that despite the global knockout the feeding centers in the brain are largely not disrupted. NT-4 KO mice do exhibit deficiencies in long-term memory, long-lasting long-term potentiation in the adult hippocampus, and loss of geniculate neurons (Patel & Krimm, 2012; Byerly & Fox, 2006). Overall, this mouse model has several potential uses, but the deficiencies of the mice should be taken into consideration when designing a behavioral study and conclusions may be limited due to potential compensations.

As previously mentioned, we did not use true wildtype mice in the current experiment. Importantly though, NT-4 HET mice show only an 8% loss of nodose ganglion neurons (Erikson et al., 1996). Furthermore, the pattern of innervation in the small intestine of HET mice was similar to that quantified in Nav1.8-Cre-tdTomato mice which have both NT-4 alleles (Serlin & Fox, 2019).

Although the most aboral sub-region of the stomach that includes the pylorus (i.e. – the region between the quantified stomach regions and the most proximal duodenum) was not measured in the present study, the lack of significant difference in amount of mucosal vagal innervation between NT-4 KO and HET in the neighboring stomach sub-region (antrum) and the reduced loss of innervation in the neighboring small intestinal sub-region (block 1) suggests there may not be a significant difference between the two conditions in the stomach region that was not quantified.

In the small intestine, there was a lack of significant loss between NT-4 KO and HET mice in the number of crypt-associated fibers. The lack of significance is most likely due to our method of bi-modal counting rather than a lack of loss. Qualitative comparison suggests a much greater loss between conditions than what was quantified (Figure 10).

Conclusion and Future Directions

Overall our findings highlight the non-static, dynamic relationship between the peripheral and central gastrointestinal vagal afferent axonal projections. Peripheral and central characterization of NT-4 deficient mice has demonstrated the utility of this mouse model in teasing apart what is communicated along the gut-to-brain vagal highway, and how the information is disseminated or converged centrally.

Previous meal pattern analyses of NT-4 deficient mice indicated unique meal pattern alterations dependent on the state (liquid, solid), energy-density of the diet, and nutrient composition (Fox et al., 2001, Byerly & Fox et al., 2006; Chi & Powley, 2007). These findings suggest that the gastrointestinal tract may utilize different mechanisms to regulate different nutrients and diet compositions. The organ-specific loss of vagal afferents allows for further investigation into what signals from the small intestine are communicated along the vagal highway.

In addition, our observed peripheral decrease and central increase of vagal afferents indicates that the relationship between the peripheral and central projections of a single pseudo-unipolar nodose cell body is dynamic. It remains a puzzling curiosity as to how a nodose ganglion cell body of a single pseudo-unipolar neuron regulates its central and peripheral receptor expression and terminal projections. Future investigations into the mechanisms of peripheral and central regulation could provide pivotal insights into the development of disordered eating by understanding how, where, and when this machinery malfunctions.

Disordered eating, such as obesity, can lead to major health issues that significantly increases early mortality and can have significant economic costs. Growing our understanding about the anatomical structure of the peripheral "feeding circuits" and how the peripheral circuits fuse with the central "feeding circuits" will help clarify what signals are communicated along the gut-brain highway and which signals are communicated locally, systemically, or reflexively. This will help us develop more efficacious, personalized treatments to a polymodal disease that is a major health problem.

LIST OF REFERENCES

Alcaino, C., Knutson, K. R., Treichel, A. J., Yildiz, G., Strege, P. R., Linden, D. R., Li, J. H., Leiter, A. B. Szurszewski, J. J., Farrugia, G., & Beyder, A. (2018). A population of gut epithelial enterochromaffin cells is mechanosensitive and requires Piezo2 to convert force into serotonin release. *PNAS, 115*, E7632-E7641.

Altschuler, S. M., Bao, X. M., Bieger, D., Hopkins, D. A., & Miselis, R. R. (1989). Viscerotopic representation of the upper alimentary tract in the rat: sensory ganglia and nuclei of the solitary and spinal trigeminal tracts. *Journal of Comparative Neurology, 28*3, 248-68.

Altschuler, S. M., Ferenci, D. A., Lynn, R. B., & Miselis, R. R. (1991). Representation of the cecum in the lateral dorsal motor nucleus of the vagus nerve and commissural subnucleus of the nucleus tractus solitarii in rat. *Journal of Comparative Neurology, 304*(2), 261-274.

Azpiroz, F. (1994). Control of gastric emptying by gastric tone. *Digestive Diseases and Sciences, 39*(12), 18s-19s.

Bai, L., Mesgarzadeh, S., Ramesh, K. S., Huey, E. L., Liu, Y., Gray, L. A., Aitken, T. J., Chen, Y., Beutler, L. R., Ahn, J. S., Madisen, L., Zeng, H., Krasnow, M. A., & Knight, Z. A. (2019). Genetic identification of vagal sensory neurons that control feeding. *Cell, 179*(5), 1129-1143.

Bellono, N. W., Bayrer, J. R., Leitch, D. B., Castro, J., Zhang, C., O'Donnell T. A., Brierly, S. M., Ingraham, H. A., & Julius, D. (2017). Enterochromaffin cells are gut chemosensors that couple to sensory neural pathways. *Cell, 170*(1), 185-198.

Berthoud, H.-R., Kressel, M., Raybould, H. E, & Neuhuber, W. L. (1995). Vagal sensors in the rat duodenal mucosa: distribution and structure as revealed by in vivo DiI-tracing. *Anatomy Embryology, 191*, 203-212.

Berthoud, H.-R., Lynn, P. A. & Blackshaw, L. A. (2001). Vagal and spinal mechanosensors in the rat stomach and colon have multiple receptive fields. *American Journal of Physiology: Regulatory Integrative Comparative Physiology, 280*(5), R1371-R1381.

Berthoud, H.-R., & Neuhuber, W. L. (2000). Functional and chemical anatomy of the afferent vagal system. *Autonomic Neuroscience, 85*(1-3), 1-17.

Berthoud, H.-R., & Powley, T. L. (1992). Vagal afferent innervation of the rat fundic stomach: morphological characterization of the gastric tension receptor. *Journal of Comparative Neurology, 319*(2), 261-276.

Blackshaw, L. A, & Grundy, D. (1990). Effects of tcholecystokinin (CCK-8) on two classes of gastroduodenal vagal afferent fibre. *Autonomic Neuroscience Research Report, 31*, 191-201.

Bonaz, B., Sinniger, V., & Pellissier, S. (2017). The vagus nerve in the neuro-immune axis: Implications in the pathology of the gastrointestinal tract. *Frontiers in Immunology, 8*, 1452.

Bradley, R. M. (2006). *The role of the nucleus of the solitary tract in gustatory processing*. 10.1201/9781420005974.

Byerly, M. S., & Fox, E. A. (2006). High-fat hyperphagia in neurotrophin-4 deficient mice reveals potential role of vagal intestinal sensory innervation in long-term control of food intake. *Neuroscience Letters, 400*(3), 240-245.

Cawthon, C. R., & de La Serre, C. B. (2018). Gut bacteria interaction with vagal afferents. *Brain Resesarch, 1693*(Pt. B), 134-139.

Chapman, I. M., Goble, E. A., Wittert, G. A., & Horowitz, M. (1999). Effects of small-intestinal fat and carbohydrate infusions on appetite and food intake in obese and nonobese men. *American Journal of Clinical Nutrition, 69*(1), 6-12.

Chambers, A. P., Sandoval, D. A., & Seeley, R. J. (2013). Integration of satiety signals by the central nervous system. *Current Biology, 23*, R379-R388.

Chi, M. M., Fan, G. & Fox, E. A. (2004). Increased short-term satiation and sensitivity to cholecystokinin in neurotrophin-4 knock-in mice. *American Journal of Physiology: Regulatory Integrative Comparative Physiology, 287*(5), R1044-R1053.

Chi, M. M., & Powley, T. L. (2007). NT-4-deficient mice lack sensitivity to meal-associated preabsorptive feedback from lipids. *American Journal of Physiology: Regulatory Integrative Comparative Physiology, 6*, R2124-R2135.

Conover, J. C., Erickson, J. T., Katz, D. M., Bianchi, L. M., Poueymirou, W. T., McClain, J., Pan, L., Helgren, M., Ip, N. Y., & Boland, P. (1995). Neuronal deficits, not involving motor neurons, in mice lacking BDNF and/or NT4. *Nature, 375*, 235-238.

Cutsforth-Gregory, J. K., & Benarroch, E. E. (2017). Nucleus of the solitary tract, medullary reflexes, and clinical implications. *Neurology, 88*, 1187-1196.

de Lartigue, G. (2016). Role of the vagus nerve in the development and treatment of diet-induced obesity. *The Journal of Physiology, 594*, 5791-5815.

de Lartigue, G., Ronveaux, C. C., & Raybould, H. E. (2014). Deletion of leptin signaling in vagal afferent neurons in hyperphagia and obesity. *Molecular Metabolism, 3*(6), 595-607.

Emond, M. H., & Weingarten, H. P. (1995). Fos-like immunoreactivity in vagal and hypoglossal nuclei in different feeding states: a quantitative study. *Physiology & Behavior, 3*, 459-65.

Erickson, J. T., Conover, J. C., Borday, V., Champagnat J., Barbacid, M., Yancopoulous, G. & Katz, D. M. (1996). Mice lacking brain-derived neurotrophic factor exhibit visceral sensory neuron losses distinct from mice lacking NT4 and display a sever developmental deficit in control of breathing. *Journal of Neuroscience, 17*, 5361-5371.

Fan, G., Egles, C., Sun, Y., Minichiello, L., Renger, J. J., Klein, R., Liu, G. & Jaenish, R. (2000). Knocking the NT4 gene into the BDNF locus rescues BDNF deficient mice and reveals distinct NT4 and BDNF activities. *Nature and Neuroscience, 4*, 350-357.

Fox, E. A. (2006). A genetic approach for investigating vagal sensory roles in regulation of gastrointestinal function and food intake. *Autonomic Neuroscience, 126-127*, 9-29.

Fox, E. A., Phillips, R. J., Baronowsky, E. A., Byerly, M. S., Jones, S., & Powley, T. L. (2001). Neurotrophin-4 deficient mice have a loss of vagal intraganglionic mechanoreceptors from the small intestine and a disruption of short-term satiety. *Neuroscience, 21*, 8602-8615.

Fox, E. A., Phillips, R. J., Martinson, F. A., Baronowsky, E. A., & Powley T. L. (2000). Vagal afferent innervation of smooth muscle in the stomach and duodenum of the mouse: Morphology and topography. *Journal of Comparative Neurology, 3*, 558-576

Gautron, L., Sakata, I., Udit, S., Zigman, J. M., Wood, J. N., & Elmquist, J. K. (2011). Genetic tracing of Nav1.8-expressing vagal afferents in the mouse. *The Journal of Comparative Neurology, 519*, 3085-3101.

Gwyn, D. G., Leslie, R. A., & Hopkins, D. A. (1985). Observations on the afferent and efferent organization of the vagus nerve and the innervation of the stomach in the squirrel monkey. *Journal of Comparative Neurology, 239*, 163-175.

Han, W., Tellez, L. A., Perkins, M.H., Perez, I. O., Qu, T., Ferreira, J., Ferreira, T. Quinn, D., Liu, Z. W., Gao, X. B., Kaelberer, M. M., Bohorquez., D., Shammah-Lagnado, S. J., de Lartigue, G., & de Araujo, I. E. (2018). A neural circuit for gut-induced reward. *Cell, 175*(3), 665-678.

Herbert, H., Moga, M. M., & Saper, C.B. (1990). Connections of the parabrachial nucleus with the nucleus of the solitary tract and the medullary reticular formation in the rat. *The Journal of Comparative Neurology, 293,* 540-580.

Holzer, P. (2007). Role of visceral afferent neurons in mucosal inflammation and defense. *Current Opinions in Pharmacology, 7*(6), 563-569.

Iwahori, Y., Ikegaya, Y., & Matsuki, N. (2002). Hyperpolarization-activated current I(h) in nucleus of solitary tract neurons: regional difference in serotonergic modulation. *Japanese Journal of Pharmacology, 88*(4), 459-462.

Kaelberer, M. M., Buchanan, K. L., Klein, M. E., Barth, B. B., Montoya, M. M., Shen, X., & Bohorquez, D. V. (2018). A gut-brain neural circuit for nutrient sensory transduction. *Science, 361*(6408): eaat5236. doi:10.1126/science.aat5236.

Keesey, R. E., & Powley, T. L. (2008). Body energy homeostasis. *Appetite, 51,* 422-445.

Kupari, J., Haring, M., Agirre, E., Castelo-Branco, G., & Ernfors, P. (2019). An atlas of vagal sensory neurons and their molecular specialization. *Cell Reports, 27,* 2508-2523.

Janssen, P., Vanden Berghe, P., Verschueren, S., Lehmann, A., Depoortere, I., & Tack, J. (2011). Review article: The role of gastric motility in the control of food intake. *Alimentary Pharmacology & Therapeutics, 33*(8), 880-894.

Lee, E. B., & Mattson, M. P. (2014). The neuropathology of obesity: Insights from human disease. *Acta Neuropathologica, 127*(1), 3-28.

Lin, C. H. (1994). Abnormal intestinal feedback in disorders of gastric emptying. *Digestive Diseases and Sciences, 39*(12), 54s-55s.

Liu, X., Ernfors, P. & Jaenisch, R. (1995). Sensory but not motor neuron deficits in mice lacking NT4 and BDNF. *Nature, 7*5, 238-241.

Madura, J. A., & DiBaise, J. K. (2012). Quick fix or long-term cure? Pros and cons of bariatric surgery. *F1000ReportsMedicine, 4,* 19.

Manning, S., Pucci, A., & Batterham, R. L. (2015). Roux-en-Y gastric bypass: Effects on feeding behavior and underlying mechanisms. *The Journal of Clinical Investigation, 125,* 939-948

Mrosovsky, N., & Powley, T. L. (1977). Set points for body weight and fat. *Behavioral Biology, 20,* 205-223.

Norgren, R., & Smith, G. P. (1988). Central distribution of subdiaphragmatic vagal branches in the rat. *Journal of Comparative Neurology, 2,* 207-223.

Palmiter, R. D. (2018). The parabrachial nucleus: CGRP neurons function as a general alarm. *Trends in Neuroscience, 41*(5), 480-293.

Paxinos, G., Huang, X., Sengul, G. & Watson, C. (2012). Organization of brainstem nuclei. In, *The human nervous system* (pp. 260-327). Amsterdam, The Netherlands: Elsevier Academic Press.

Peters, J. H., Gallaher, Z. R., Ruy, V& ., Czaja, K. (2014). Withdrawal and restoration of central vagal afferents within the dorsal vagal complex following subdiaphragmatic vagotomy. *Journal of Comparative Neurology, 521,* 3584-3599.

Phillips, R.J., Powley, T. L. (1996). Gastric volume rather than nutrient content inhibits food intake. *American Journal of Physiology. 271,* R766-R769.

Phillips, R. J., & Powley, T.L. (1998). Gastric volume detection after selective vagotomies in rats. *American Journal of Physiology. 274*(6), R1626-R1638.

Pirnik, Z., Bundzikova, J., Holubova, M., Pychova, M., Fehrentz, J. A., Martinez, J., Zelezna, B., Maletinska, L., & Kiss, A. (2011). Ghrelin agonists impact on Fos protein expression in brain areas related to food intake regulation in male C57BL/6 mice. *Neurochemistry International, 6,* 889-895.

Powley, T. L., Chi, M. M., Baronowsky, E. A., & Phillips, R.J. (2005). Gastrointestinal tract innervation of the mouse: Afferent regeneration and meal patterning after vagotomy. *American Journal of Physiology, 289*(2), R563-R574.

Powley, T. L., Spaulding, R. A., & Haglof, S. A. (2011). Vagal afferent innervation of the proximal gastrointestinal tract mucosa: Chemoreceptor and mechanoreceptor architecture. *Journal of Comparative Neurology, 4,* 644-660

Roman, C. W., Derkach, V. A., & Palmiter, R. D. (2016). Genetically and functionally defined NTS to PBN brain circuits mediating anorexia. *Nature Communications, 7*, 11905.

Schwartz, G. J., Salorio, C .F., Skoglund, C., & Moran, T. H. (1999). Gut vagal afferent lesions increase meal size but do not block gastric preload-induced feeding suppression. *Regulatory, Integrative, and Comparative Physiology, 276*(6), R1623-R1629.

Serlin, H. K., & Fox, E. A. (2019). Abdominal vagotomy reveals a majority of small intestinal mucosal afferents labeled in nav1.8cre-rosa26tdTomato mice are vagal in origin. *Journal of Comparative Neurology, 528,* 816-839.

Shapiro, R. E., & Miselis, R. R. (1985b). The central organization of the vagus nerve innervating the stomach of the rat. *Journal of Comparative Neurology, 23*, 473-488.

Sternson, S. M. & Eiselt, A. K. (2017). Three pillars for the neural control of appetite. *Annual Review of Physiology, 79*, 401-423.

Stirling, C. L., Forlani, G., Baker, M. D., Wood, J. N., Matthews, E. A., Dickenson, A. H., Nassar, M. A. (2005). Nociceptor-specific gene deletion using heterozygous Nav1.8-Cre recombinase mice. *Pain, 113*, 27-36.

Sugawara, K., Isaza, J., Woodward, E. R., & Dragstedt, L.R. (1969). The short-term effect of vagotomy of gastric motility. *The Archives of Surgery*, *99*(1), 1-5.

Wang, F. B., & Powley, T. L. (2000). Topographic inventories of vagal afferents in gastrointestinal muscle. *Journal of Comparative Neurology, 421*, 302-324.

Williams, E. K., Chang, R. B., Strochlic, D. E., Umans, B. D., Lowell, B. B., & Liberles, S. D. (2016). Sensory neurons that detect stretch and nutrients in the digestive system. *Cell, 166*, 209-221.

Zhuo, H., Ichikawa, H., & Helke, C.J. (1997). Neurochemistry of the nodose ganglion. *Progress in Neurobiology., 52*, 79-107.